DUAL-FREQUENCY OPTOELECTRONIC OSCILLATOR AND ITS APPLICATION IN TRANSVERSE LOAD SENSING

by

Fanqi Kong

A Thesis
Submitted to the Faculty of Graduate and Postdoctoral Studies
in Partial Fulfillment of the Requirements
for the Degree
Master of Applied Science

Ottawa-Carleton Institute of Electrical and Computer Engineering
School of Electrical Engineering and Computer Science
University of Ottawa

Master of Applied Science (2014)

Electrical and Computer Engineering

University of Ottawa

Ottawa, Ontario, Canada

TITLE:

Dual-frequency Optoelectronic Oscillator and Its Application in Transverse Load Sensing

AUTHOR: Fanqi Kong

SUPERVISOR: Professor Jianping Yao

TOTAL PAGES: xiv, 86

ABSTRACT

In this thesis, dual-frequency optoelectronic oscillators (OEOs) and their applications to transverse load sensing are studied. Two configurations of dual-frequency OEOs are proposed and investigated. In the first configuration a polarization-maintaining phase-shifted fiber Bragg grating (PM-PSFBG) is employed in the OEO loop to the generation of two oscillating frequencies. The beat between the two oscillating frequencies is a function of the load applied to the PM-PSFBG, which is used in transverse load sensing. To avoid the frequency measurement ambiguity, a second configuration is proposed by coupling a dual-wavelength fiber laser to the dual-frequency OEO. A single tone microwave signal with the frequency determined by the birefringence of the grating is generated in the OEO and is fed into the fiber ring laser to injection lock the dual wavelengths. The sensitivity and the resolution are measured to be 9.73 GHz/(N/mm) and 2.06×10^{-4} N/mm, respectively. The high stability of the single-tone microwave signal permits accurate measurement, while the frequency interrogation allows an ultra-high speed demodulation.

RÉSUMÉ

Dans cette thèse, des oscillateurs optoélectroniques bi-fréquence et des applications à détection de pression transversale sont étudiés. Deux configurations d'oscillateurs optoélectroniques bi-fréquence sont proposés et étudiés. Dans la première configuration, un réseau déphasée maintenant la polarisation à fibre de Bragg est utilisée dans la boucle d'oscillateur optoélectronique pour générer deux fréquences d'oscillation. Le battement entre les deux fréquences d'oscillation est une fonction de la pression appliquée au réseau, qui est utilisé dans la détection de la pression transversale. Pour éviter l'ambiguïté dans la mesure de fréquence, une seconde configuration est proposée par le couplage d'une double longueur d'onde laser à fibre à l'oscillateur optoélectronique bi-fréquence. Un signal micro-onde à tonalité unique est généré avec sa fréquence déterminée par la biréfringence du réseau de Bragg. Il est introduit dans le laser à fibre en anneau à injection pour verrouiller les deux longueurs d'onde. La sensibilité et la résolution mesurées sont 9,73 GHz/(N/mm) et $2{,}06\times10^{-4}$ N/mm, respectivement. La grande stabilité du signal micro-onde à tonalité unique permet une mesure précise, alors que l'interrogatoire de fréquence permet une démodulation d'ultra-rapide.

TABLE OF CONTENTS

LIST OF PUBLICATIONS

Much of the author's research in this thesis, Chapter 3 and Chapter 4, has previously appeared in publications [J1] and [J3], respectively:

Peer-Reviewed Journal Papers (as the first and second author)

[J1] F. Kong, W. Li and J. P. Yao "Transverse load sensing based on a dual-frequency optoelectronic oscillator," *Opt. Lett.*, vol. 38, no. 14, pp. 2611-2613, Jul. 2013.

[J2] W. Li, F. Kong, and J. P. Yao, "Arbitrary microwave waveform generation based on a tunable optoelectronic oscillator," *J. Lightw. Technol.*, vol. 31, no. 23, pp. 3780-3786, Dec. 2013.

[J3] F. Kong, B. Romeira, J. Zhang, W. Li and J. P. Yao, "A dual-wavelength fiber ring laser incorporating an injection-coupled optoelectronic oscillator and its application to transverse load sensing," *J. Lightw. Technol.*, vol. 20, no. 9, pp. 1784-1793, May. 2014.

[J4] B. Romeira, F. Kong, W. Li and J. P. Yao, "Broadband Chaotic Signals and Breather Oscillations in an Optoelectronic Oscillator Incorporating a Microwave Photonic Filter," *J. Lightw. Technol.*, vol. 32, no. 20, pp. 3933-3941, Oct. 2014.

Peer-Reviewed Conference Processings

[C1] W. Li, F. Kong, and J. P. Yao, "Phase-coded microwave waveform generation based on a tunable optoelectronic oscillator," MWP2013, 28-30 October 2013, Alexandria, VA, USA.

LIST OF ACRONYMS

D

DSB+C	double sideband + carrier
DSP	digital signal processing

E

EMI	immunity to electromagnetic interference
EA	electrical amplifier
EDFA	erbium-doped fiber amplifier
ESA	electrical spectrum analyzer

F

FBG	fiber Bragg grating
FSR	free spectral range
FP-LD	Fabry-Pérot laser diode

L

LCFBG	linear chirped fiber Bragg grating

M

MWP	microwave photonic
MPF	microwave photonic filter
MZI	Mach-Zehnder interferometer
MZM	Mach-Zehnder modulator

O

OBPF	optical band pass filter
OC	optical circulator
OEO	optoelectronic oscillator
OSA	optical spectrum analyzer

OVA	optical vector analyzer

P

PC	polarization controller
PD	photodetector
PM	phase modulator
PM-IM	phase modulation to intensity modulation
PolM	polarization modulator
Pol	polarizer
PMF	polarization-maintaining fiber
PM-PSFBG	polarization-maintaining phase-shifted fiber Bragg grating
PSFBG	phase-shifted fiber Bragg grating

R

RF	radio-frequency

S

SBS	stimulated Brillouin scattering
SNR	signal to noise ratio
SSB+C	single sideband +carrier
SSB-IM	single sideband intensity modulation

V

VNA	vector network analyzer

LIST OF FIGURES

Number *Page*

ACKNOWLEDGEMENTS

First and foremost I offer my sincerest gratitude to my supervisor, Professor Jianping Yao, for providing me with strong academic atmosphere, state-of-the-art research facilities and meticulous guidance. Also for the freedom he granted to me during my work in his lab and his encouragement helping me to overcome frustrations. I would never complete these research works without his support.

I am grateful to my senior colleagues: Dr. Muguang Wang, who patiently and thoroughly standardized my every basic experiment skills even started from how to connect RF cables; Dr. Wangzhe Li, who was always willing to take time to coach me experimental techniques or to fix the amplifiers; Jiejun Zhang, whose valuable insights on my experimental details helped me to complete this work.

I am also indebted to Dr. Bruno Romeira for being patient and inspirational, and for teaching me the importance of using curiosity as the driving force behind research. Invaluable lessons I learnt from him regarding the log book will definitely go along with my career and defense the ethics of research. It might be the worst coffee in the afternoon but most memorable experience sharing ideas, listening those new physics terms and enjoying the priceless sunshine in Ottawa with him.

Additionally, I would like to thank all my colleagues of the Microwave Photonics Research Laboratory for creating a friendly and supportive environment. This includes (in alphabetical order) Xiang Chen, Yang Chen, Wentao Cui, Nasrin Ehteshami, Liang Gao, Weilin Liu, Yinqing Pei, Hiva Shahoei, Tong Shao and Weifeng Zhang.

Finally, I would thank Susie, for her amazing ironing skills and the hand-pressed, crease-free shirts she put on me.

DEDICATION

I dedicate my dissertation work to my loving mother, Mrs. Yandi Wang, and father, Mr. Tianyi Kong, for their continuous love and for always believing in me by offering absolute supports to my decisions. I could not have made it here without them.

‘Ce qui embellit le désert, c'est qu'il cache un puits quelque part.’

What makes the desert beautiful is that somewhere it hides a well.

— Antoine de Saint-Exupéry

Chapter 1

Introduction

1.1 Background

Microwave photonics (MWP) has been defined as the study of photonic devices operating at microwave frequencies and their application to microwave and optical systems [1-3]. Its initial rationale was to use the advantages of optical communication system to transmit the microwave signals over long distance through the low loss telecom optical fibers [4-6]. Besides the signal transmission, spectrum filtering [7-10], frequency conversion [11-13], mathematical operations [14-17], the generation of ultra-wideband [18] and ultra-stable [19] microwave signals can also be accomplished by using optical methods. The involvement of photonics offers unrivaled advantages to the microwave technology, including: low loss, high frequency and immunity to electromagnetic interference. Conversely, MWP is also succeeding in incorporating a variety of techniques used in microwave engineering to improve the performance of photonic communication networks and systems. The high speed processing, stable operating and low cost electronic devices can significantly benefit the photonic systems. For example, in modern communication systems, the digital signal processing (DSP) technology enables post compensation to the distorted signals transmitted through optical links [20-22], which greatly enlarges the capacity and reduces the cost of optical communication systems.

To further exploit the ultra-broad bandwidth of optical systems, numerous techniques have been developed to generate high-quality microwave signals at high frequency, for instance, through optoelectronic feedback [24, 25], optical feedback [26-29], optical injection [30-33]. Among the various techniques developed, the use of an optoelectronic

oscillator (OEO) [23] is considered as one of the promising solutions to generate high quality microwave signals. The OEO is an oscillator with a hybrid structure consisting of an optical path and an electrical path in the loop, which produces microwave signals or intensity modulated lightwave signals. In the OEO loop, light from the output port of an electro-optic modulator is detected by a photodetector and then is amplified, filtered, and fed back to the electrical input port of the modulator. If the modulator is properly biased and the small signal gain is properly chosen, the optoelectronic oscillation will be sustained. The high frequency microwave signal is produced through heterodyning the optical carrier and its sidebands at a photodetector. Taking advantage of the low loss transmission in the optical fiber, the optoelectronic loop can form a high Q cavity with long optical delay and generate single tone microwave signal with ultra-low phase noise [34]. It has been reported that the phase noise can be suppressed down to as low as -150 dBc @10 kHz using an injection configuration [35] and the compact commercialized product can reach -140dBc @10kHz [36].

As an oscillator, an OEO can operate at various states with different gain and initial conditions. That makes the OEO an ideal device in systematic studies and numerous engineering applications. Besides generating a high-quality single tone microwave signal, the OEO has also been intensively investigated in chaotic signal generation for nonlinear dynamic system studies [37, 38], encoding signal phase for radar application [39] and clock recovery in high speed optical telecommunications [40, 41].

The particular device and its system response are significantly influenced by the mode selection scheme. Several mode selection configurations have been developed to assist OEO in improving their performance and enhancing their functions. For example, a dual-loop configuration is proposed to realize a more stable single tone operation by employing

a high Q cavity with two optical paths of different lengths [42]: The short optical loop ensures a relatively large free spectrum range (FSR), whereas the long one creates as an optical comb-like filter with narrow bandwidth for each passband. Therefore the OEO can generate microwave signals with low phase noise. On the contrary, a broad bandpass microwave filter with distinguishable low and high cut-off frequencies is applied into the delay loop, in which a chaotic oscillation was observed [43, 44]. The hybrid state of simultaneous fast scale chaos and slow scale periodicity emerged subsequently to a sequence of Hopf bifurcations. In a sense, the neuronal-like signal generation in the OEO opens a realistic route to study the neuron science and complex system question with a bench-top microwave photonic setup.

Besides aforementioned different types of mode selection schemes in the electrical domain, the mode selection can also be accomplished optically, which potentially enhances its frequency tunability and reconfiguration ability by taking advantages of the large bandwidth provided by the photonic technologies. Several research teams have reported their approaches to form OEOs through optical filtering, which can be grouped into three categories: nonlinear effect based optical filtering, fiber grating-based optical filtering and optical resonator-based filtering.

As an example of the nonlinear effects-based schemes, the optical mode selection through a stimulated Brillouin scattering (SBS)-based optical filter was proposed by Yao in 1997 [45]. Taking advantage of a narrow backward gain linewidth (~10 MHz) of the anti-Stokes process, a single sideband is selected and enhanced through the SBS effect. The enhanced sideband frequency is 12.8 GHz lower than that of the optical carrier. Regenerating the beat signal at a photo detector (PD), an oscillating microwave signal was produced experimentally with a fixed frequency at 12.8 GHz. In order to achieve a large

tunable range in frequency, another approach implemented by Li with a linear chirped fiber Bragg grating (LCFBG)-assisted microwave photonic filter realized tunability from 6.5-11.5 GHz [46]. With the improved fabrication technology for fiber Bragg gratings (FBG), an MWP bandpass filter with even narrower bandwidth (~30 MHz) can be achieved by introducing a phase shift in a FBG. This enables the optical filtering in OEO with a phase shifted fiber Bragg grating (PSFBG). Promising results [47] had shown to realize the largest ever tunable range in an OEO of 3-28 GHz with the PSFBG-based setup. Alternatively, frequency tunable OEO can also be implemented with optical resonator based filter. For this type of schemes, a demonstration has been performed by Pan [48], through injecting the light signal into a Fabry-Pérot laser diode (FP-LD) under its emitting threshold, where single sideband signal was enhanced within one of the narrow linewidth resonances of the FP-LD. A tuning bandwidth of around 4 GHz of the microwave signal is reported, which was severely limited by the FSR of the etalon. Another experiment conducted with a higher finesse (up to 1000) Fabry–Pérot etalon conducted by Ozdur [49], reveals another potential application to the OEO with optical filters. Instead of having a stabilized single longitudinal mode operation, however, another inspiring phenomenon is reported that the output microwave frequency accordingly shifted with the frequency drift of the optical pump laser. Such microwave frequency drift was used to measure the optical frequency stability of the pump laser. Since the variation of optical parameters can be monitored by demodulating electrical signal, the OEO could be designed as a sensor system at the interface between the electrical and optical domain.

Based on the previous investigation on the FBG-based OEO, the FBG, which has been widely used in optical sensing, can take over the role of etalon reported in [49]. Consequently, a femtometer resolution for the axial strain induced stretch sensor has been achieved [50] through a similar setup in [47] by placing the PSFBG onto a micro

translation stage. These results illustrate that OEO is a competitive configuration among ultra-high sensitivity sensing systems which takes advantages from both the optical and the electrical domains. In this manner, the OEO served as an innate medium bridging between the optical sensing and electrical detection.

The inherent advantages of fiber-optic sensors, including low loss, small size, light weight, high sensitivity, and immunity to electromagnetic interference, push them to be widely applied in numerous fields such as structural health monitoring [51, 52], medical treatment [53] and pipeline security monitoring [54]. The sensing information encoded in an FBG due to the structural distortion [55, 56] can be interrogated through measuring its optical property. The birefringence, in particular, as a key optical property describing the anisotropy of an FBG along the two orthogonal polarization directions in terms of the refractive indices, provides an important measurement to the lateral external disturbance such as bending, pressing and twisting [57, 58]. Among the various physical quantities that can be measured through monitoring the change of the birefringence, the transverse load is a vital parameter in structural health monitoring, which can be ideally measured through the non-axisymmetric load induced birefringence [59]. However, the lateral force-induced refractive index change is very small, thus a specially designed interrogation technique must be employed to demodulate the weak sensing information.

One possible solution is to use frequency interrogation techniques [60, 61] to demodulate the structure distortion induce Bragg wavelength shift in the electrical domain. From the information interrogation point of view, the shifting of the microwave frequency offers a path to inspect changes to certain physical quantities in the OEO. In other words, the external disturbance acting on the sensor probe is encoded in the frequency shift of the output microwave signal. Comparing to those commonly used optical domain interrogation

techniques for fiber-optic sensors, frequency interrogation is a faster, more accurate but less expensive solution, accompanied with mature real-time frequency detection techniques [62] and digital signal processing devices. Typically, fast Fourier transform requires about 10 to 22 clock cycles/sample in a 32 bit DSP, corresponding to a throughput of about 4.5M to 10M samples/second with a 100 MHz clock.

1.2 Research objectives and contributions

In the previous research, the OEO operating principles have been investigated using different control factors, including the gain, the delay and the frequency filtering. However, as one of the key parameters of a light wave, the property of the polarization in the OEO system has never been explored. We endeavor to demonstrate the stable operation of the proposed dual-frequency OEO and develop a transverse load sensor system by interrogating its output microwave signal to achieve high-speed and high-accuracy signal demodulation.

The main contributions of this thesis include:

1) **The development of a novel a transverse load fiber-optic sensor employing frequency interrogation based on the dual-frequency OEO.**

A further experiment, where standard referenced external disturbances (the planar transverse load) are introduced onto the polarization maintaining phase-shifted fiber Bragg grating (PM-PSFBG), revealed the capability of demodulating sensing signal from the beat between the two Eigen-mode oscillations. The sensitivity and the minimal detectable load are measured to be as high as 9.73GHz/ (N/mm) and 2.6×10^{-4}N/mm, which extends its potential application to ultra-high sensitivity and fast sensing information interrogation.

2) **The proposal of a fiber laser coupled dual-frequency OEO and eliminating the ambiguity in the frequency measurements.**

In order to enhance the output power of the microwave signals and eliminate the ambiguity in the frequency measurement in the previous system, we removed the pump laser by embedding a self-designed fiber ring laser, in which the PM-PSFBG is

functionalized as an optical filter in its transmission band. The compatibility to the dual wavelength laser imprints the increasing stability to the system by forcing the two polarized modes to be phase locked and talk to each other. To characterize this novel system coupled by the OEO and the fiber ring laser, we analytically derived the self-consistency condition in terms of the complex amplitudes of both electric fields along two orthogonal polarization states. Considering real sensing application aspect, allowing only the beat frequency to survive in the loop, such structural modification effectively avoids the ambiguity in the previously proposed OEO based sensor.

1.3 Organization

The thesis consists of 5 chapters. In Chapter 1, a brief introduction to the photonic microwave generation is presented, underlining with different architectures of OEOs and their cross-disciplinary applications in optical sensing. After reviewing the challenges remained in the current fiber-optic sensing information interrogation, the motivation is given and the main contributions are described.

In Chapter 2, an overview of some of the key techniques and devices in employed in the dual-frequency OEO system are provided.

In Chapter 3, a novel configuration of dual-frequency OEO with a birefringent phase-shifted FBG (PSFBG) is proposed and implemented. A proof of concept demonstration is then performed by demodulating the external transverse stress from the frequency of the beat signal.

In Chapter 4, a refined scheme, embedded with a fiber ring laser, is described for the first time both theoretically and experimentally. An iterative model based on the self-consistence condition is derived, to describe this novel type of system. Experimentally, the single tone operation at the beat frequency is presented. In addition, a similar sensing experiment is performed with more position control and detailed results with increasing reliability are discussed.

Final conclusions are drawn in Chapter 5, along with some perspectives for the future work.

Chapter 2

Technical Overview

The dual-frequency optoelectronic oscillator is essentially a conventional optoelectronic oscillator equipped with a polarization-dependent optical filter. The new type of the microwave photonic filter previously developed in our group based on PSFBG paved the way to embed two orthogonally polarized light waves in an OEO and to study the more complex behaviours in OEOs with increased bandwidth and tunability.

In this chapter, several key techniques and devices employed in the dual-frequency optoelectronic oscillator, such as optoelectronic oscillators, fiber Bragg gratings and optical birefringence, are presented and reviewed. We focus on characterizing the polarization-dependent behaviour of the microwave photonic filter based on a polarization-maintaining fiber Bragg grating. The polarization property of the filter distinguishes two orthogonally polarized modes in the optical fiber and enables the transverse load sensor probe design.

2.1 Optoelectronic oscillators

2.1.1 Basic configurations

The concept of optoelectronic oscillator was first proposed by Yao in 1996 [23]. It utilized the transmission characteristics of a modulator together with a fiber-optic delay line to convert pump light energy into stable, spectrally pure microwave reference signals. The essence of the work highlights forming a high Q cavity, by taking advantage of low transmission loss (~0.2dB/km @1550nm) and long delay (~10s μs) in the optical fiber. A similar delayed system with optoelectronic feedback attracted a lot of interest and has already been inspected in nonlinear delayed systematic research [63]. Fig. 1 shows the basic construction of an OEO.

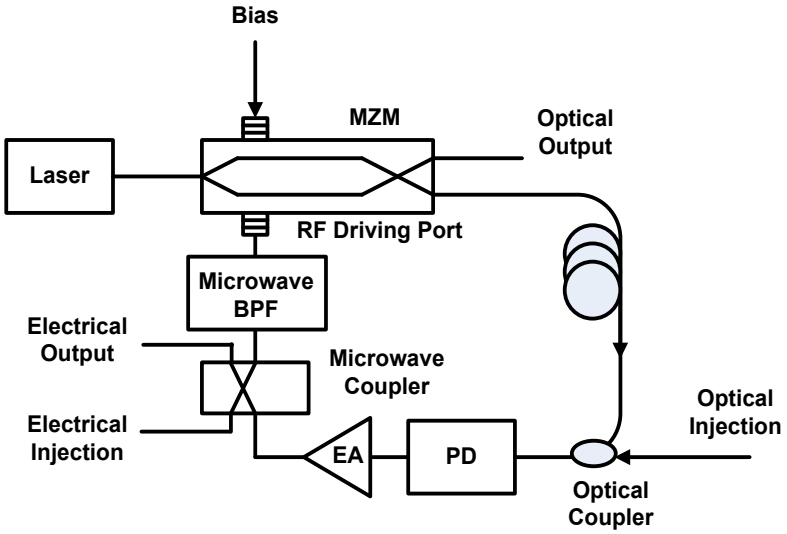

Fig. 2-1 Device description of the OEO. Microwave-BPF: microwave - band pass filter; PD: photo detector; EA: electrical amplifier; MZM: Mach-Zehnder modulator

In a free run OEO system the optical carrier or the pump light is initially modulated by noises produced by the electrical units in the system. Then, after a long distant transmission

within the optical delay line, the modulated optical light wave is converted to electrical voltage signal by a photo detector. The electrical voltage signals, which contain broadband frequencies, are produced by the noises of any devices inside the loop. Such voltage signals are amplified by the electrical amplifiers (EA) and then loaded through a Mach-Zehnder modulator (MZM) onto the optical carrier, provided by a CW pump laser. Thus, the electrical signals are converted back into an intensity-modulated optical signal, completing this opto-electronic hybrid loop.

The typical MZM structure is shown in Fig. 2-1, which consists of two arms. The incoming optical signal is split equally and is sent down two different optical paths. After a few centimeters, the two paths recombine, causing the optical waves to interfere with each other. If the phase shift between the two waves is 0°, then the interference is constructive and the light intensity at the output is high (on state); if the phase shift is 180°, then the interference is destructive and the light intensity is zero (off state). The phase shift, and thus the output intensity, is controlled by changing the delay through one or both of the optical paths by means of the electro-optic effect. This effect occurs in some materials such as lithium niobate (LiNbO3). The transmission function in terms of the electrical voltage is usually given by

$$P_{\text{out}} = \frac{\alpha_{\text{MZM}}}{2}\left[1 - \kappa \sin\left(\frac{\Delta V}{V_{\pi}}\right)\right] P_{\text{in}} \ , \tag{2-1}$$

where P_{out} is the output power , α_{MZM} is the losses when light coupled in/out of MZM, κ is the extinction ratio, ΔV is the different of the voltage applied on to the two paths, V_{π} is the half-wave voltage of MZM and P_{in} is the input power.

Taking the output and launching it into a long distance but low loss optical fiber, the microwave signal will be deposited in the optical domain with a low damping ratio. Then, the microwave signal modulated on the optical carrier is recovered by the photo detector and completes a round trip. The voltage of the regenerated signal at a particular frequency is given by

$$V_{\text{out}} = I_{\text{p}} L = \eta e P / h\nu L = PR(\lambda) L, \tag{2-2}$$

where I_{p} is the photo current generated by the photo diode, L is the load resistance, η represents the quantum efficiency, $R(\lambda)$ is the responsivity depending on the incident wavelength λ, P is the power of the incident light. Ideally, this linear process, within the cutoff and threshold frequency, will not induce any change on the waveform but the intensity. To start oscillating or generate a single frequency microwave signal, an electrical amplifier and/or a microwave frequency band pass filter can be inserted into the electrical path, which enhances the power of signals and selects the frequency we intend to generate, respectively. Alternatively, both the electrical and optical injection ports are designed in the loop, in order to have a better control over the system. The injected small signal can also be employed as a perturbative probe in order to study the dynamics of this delayed feedback system.

2.1.2 Threshold condition

Within the passband of the electrical filter, the frequency components whose gain can compensate its losses will have the potential to oscillate. Considering the signal is extracted from initial noises in the system, the criteria for oscillation turn out to be that the small signal gain after one round trip is greater than unity. By substituting Eq. (2-1) into Eq. (2-2),

such building-up process in round trip can be described in terms of the input voltage to the MZM by

$$\begin{aligned} V_{\text{out}} &= RP_{\text{out}}LG_{\text{A}} \\ &= R\frac{\alpha_{\text{MZM}}}{2}\left[1-\kappa\sin\left(\frac{\Delta V}{V_\pi}\right)\right]P_{\text{in}}LG_{\text{A}} \\ &= R\frac{\alpha_{\text{MZM}}}{2}\left[1-\kappa\sin\left(\frac{V_{\text{in}}+V_{\text{bias}}}{V_\pi}\right)\right]P_{\text{o}}LG_{\text{A}} \end{aligned}, \tag{2-3}$$

where R is the responsivity of PD, L is the load resistance, G_{A} is the gain of the amplifier, and P_{o} is the output power of the pump laser. Both the bias and the driving voltages contribute to the phase difference between the two paths.

The small signal gain G_{s} can be obtained by

$$G_{\text{s}} = \left.\frac{dV_{\text{out}}}{dV_{\text{in}}}\right|_{V_{\text{in}}=0} = -\frac{\kappa\pi\alpha P_{\text{o}}RLG_{\text{A}}}{2V_\pi}\cos\left(\frac{\pi V_{\text{bias}}}{V_\pi}\right). \tag{2-4}$$

The oscillation threshold can be derived based on G_s>1, assuming bias is set to be zero:

$$\alpha P_{\text{o}}RLG_{\text{A}} > \frac{2V_\pi}{\pi}\ . \tag{2-5}$$

The left side is the output voltage of a trans-impedance amplifier. This reveals that the OEO is pumped by both optical source (the pump laser P_{o}) and electrical amplification (the electrical power amplifier G_{A}). In other words, if the parameters are chosen properly and losses are optimized, the electrical amplification is not necessary in the loop. Such all-

optical pumped OEO configuration [64] can significantly reduce the phase noise by eliminating contribution from the thermal noise of the amplifiers.

2.1.3 Longitudinal modes

Similar to fiber ring laser architectures, the resonance cavity (the optoelectronic feedback loop) of the OEO also forms its intrinsic mode selection mechanism: The longitudinal modes, corresponding to the frequencies of the wave which are reinforced by constructive interference after many round trips along the ring loop, will be mostly transmitted; while all other frequencies are suppressed by destructive interference.

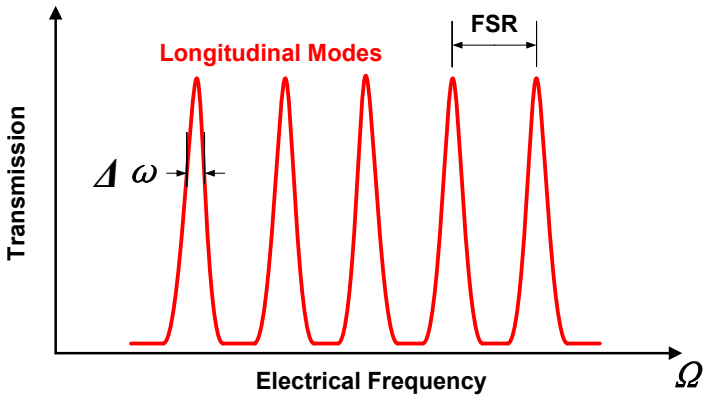

Fig. 2-2 The transmission spectrum of a ring resonator. FSR: free spectrum range; $\Delta\omega$: the linewidth of longitudinal modes.

For resonance to take place, the following resonant condition must be satisfied:

$$l_{\text{eff}} = m\lambda = \frac{2\pi c}{\omega} m\,. \tag{2-6}$$

Here λ is the resonant wavelength, ω is the angular frequency and m is the mode number of the ring resonator. Eq. (2-6) illustrates that in order for the signal to interfere constructively

after rounds along the ring delay line, the length of the feedback loop must be an integer multiple of the wavelength of the microwave signal. As such, the mode number must be a positive integer for resonance to take place. When the incident light contains multiple wavelengths (such as in OEO cases, noise modulated signal), the constructive interference wavelengths will be able to pass through the ring resonator fully while other wavelengths will be attenuated depending on their detuned frequency, as shown in Fig. 2-2. The spacing between two adjacent modes, usually noted as the free spectrum range (FSR) of the ring resonator, can be derived from Eq. (2-6):

$$\mathrm{FSR} = \frac{2\pi c}{l_{\mathrm{eff}}} = \frac{2\pi c}{n_{\mathrm{eff}} l_{\mathrm{phy}}} \quad . \tag{2-7}$$

It can be seen from Eq. (2-7) that the mode spacing is constant as long as the physical loop is chosen. Typically the physical length of OEOs, including the optical and electrical paths, can reach up to several kilometres which correspond to an FSR only about 100s kHz. All such dense longitudinal modes which fulfill the gain condition will have the potential to be excited, shown in Fig. 2-3(a). The mode hopping and multimode behavior have been observed when no additional filter [65] or a relatively large bandwidth filter [66] is inserted in the OEO loop.

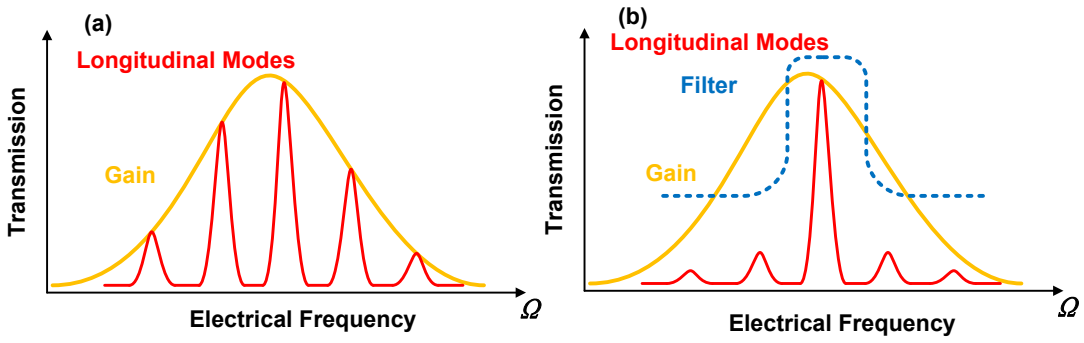

Fig. 2-3 (a) The transmission spectrum with electrical amplifiers with a certain passband. (b) The transmission function of the OEO loop with a narrow electrical filter, which selects only one longitudinal mode.

To achieve a single mode operation, it is necessary to apply additional mode selection units to assist the oscillation: both the electrical amplifier and the filter play a role to select the particular frequencies which we are interested in to go above the threshold and suppress the side modes which are less desired. As can be seen from Fig. 2-3(a), the longitudinal mode is enveloped by the gain profile of electrical amplification or the optical active medium. Furthermore, the side modes are suppressed by the narrow passband of the electrical filter Fig. 2-3(b). Only the frequency locating inside the passband of the filter will fulfill the oscillation condition and drive the electro-optic modulator again. Making use of this controllable characteristic, on one hand, the profiles of both the gain medium and the filter can be designed to determine the oscillation frequency. By controlling the characteristic parameters, OEO can serve as tunable microwave sources. On the other hand, the output signal provides a good estimate to the changes occuring in the devices. That is, the OEO has the potential to be designed as a sensor system.

2.2 Fiber Bragg Gratings

2.2.1 Types of FBGs

The fiber Bragg grating is a type of periodic micro structure along the core of optical fibers. The periodically modulated refractive index forms a series of dielectric mirrors along the light propagation direction, which can reflect the light with particular wavelength depending on the design of the structure. An FBG can therefore be used as an inline optical filter to block certain wavelengths, or as a wavelength-specific reflector. The first in-fiber Bragg grating was demonstrated by Dr. Hill in 1978 [67]. Initially, the gratings were fabricated using a standing wave produced by a visible laser propagating along the fiber core. In 1989, Dr. Meltz et al. [68] demonstrated the much more flexible transverse holographic inscription technique where the laser illumination came from the side of the fiber. This technique uses the interference pattern of two angled UV beams to create the periodic structure of the fiber Bragg grating. Another commonly used approach is using the diffraction pattern of a special phase mask grating made of silica glass [69], shown in Fig. 2-4.

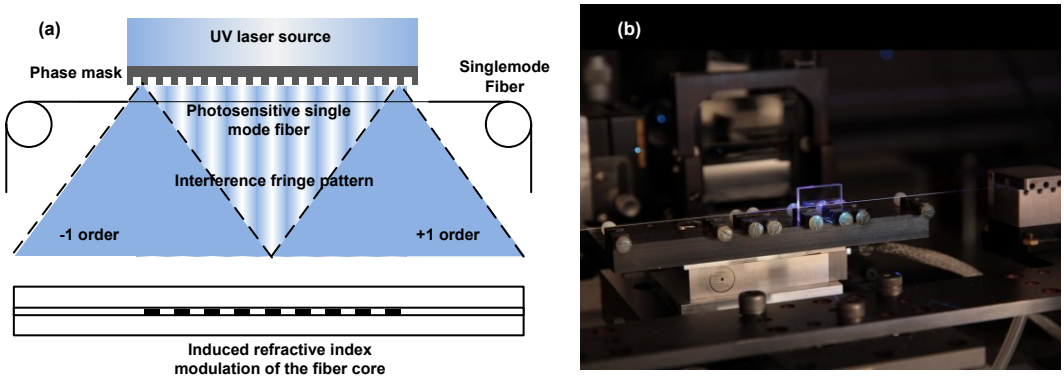

Fig. 2-4(a) The schematics of fabricating FBG by using phase mask technique. (b) The FBG fabrication facilities.

The masking technique make it possible to manufacture more complex FBG strucutre besides the uniforms. Several types of the FBG are listed in Fig. 2-5, including the uniform FBG, the chirped FBG, the sampled FBG, the phase-shifted FBG and the tilted FBG.

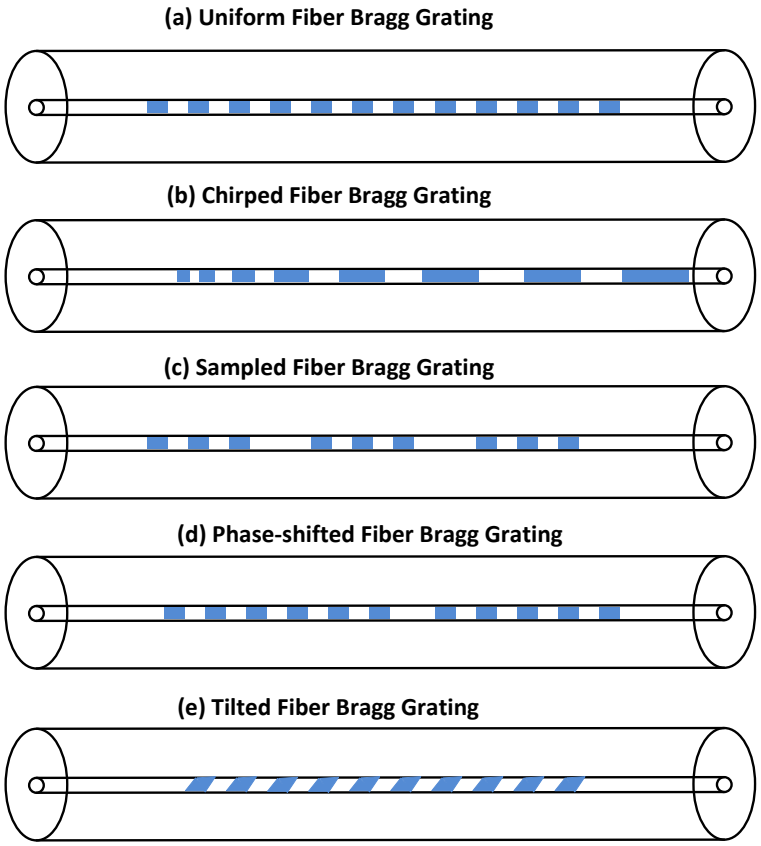

Fig. 2-5 Different types of FBGs. (a) uniform FBG; (b) Chirped FBG; (c) Sampled FBG; (d) Phase-shifted FBG; (e) Tilted FBG

For a uniformed FBG, shown in Fig. 2-5(a), the reflected central wavelength is given by Eq. (2-8) in an infinitesimally weak grating ($\delta n_{\text{eff}} \rightarrow 0$), with a period Λ.

$$\lambda_B = 2n_{\text{eff}}\Lambda \tag{2-8}$$

where Λ is the grating period, λ_B is the Bragg wavelength, and n_{eff} is the effective refractive index of light in the fiber. Essentially, the condition means that the wavenumber of the grating matches the difference of the wave vectors of the incident and reflected waves. In that case, the complex amplitudes corresponding to the reflected field contributions from different parts of the grating are all in phase so that they can add up constructively; this is a kind of phase matching. Even a weak index modulation (with an amplitude of e.g. 10^{-4}) is sufficient for achieving nearly total reflection, if the grating is sufficiently long (e.g., a few millimeters).

More functions can be achieved by other types of FBGs: A chirped FBG, shown in Fig. 2-5(b), has a wider reflection spectrum, and each wavelength component is reflected at different positions, which results in a time delay difference for different reflected wavelengths. A sampled FBG, Fig. 2-5(c), is produced by sampling a uniform FBG, which can reflect multiple wavelength components with identical wavelength spacing when the sampling function is uniform. The use of a non-uniform sampling function, such as a sampling function with increasing or decreasing spacing, a reflection spectrum arbitrary spectral response in the 1st order spectral channel can be generated. A phase-shifted FBG, shown in Fig. 2-5(d), is written with a discrete phase jump in the middle of the grating, which break the phase matching between the reflected light from the sub-grating before and after the phase shifted point. The backwards reflected light waves interfere destructively and form an ultra-narrow window at its Bragg wavelength to tunnel through the grating. A tilted FBG, shown Fig. 2-5(e), could couple the forward propagating core mode to the backward propagating core mode and a backward propagating cladding mode. Different types of gratings have been employed for different applications, such as in sensing [70, 71], spectral filtering [72], and dispersion compensation [73], according to their specific attributes.

2.2.2 Microwave photonics filter based on a PSFBG

Among various complex structured FBG, the PSFBG has been intensively investigated, for its ultra-narrow transmission band (around tens of femto-meters), in laser architectures [74, 75], optical switching [76, 77] and optical communication systems [19, 78]. The PSFBG also attracts a lot of interest for microwave photonics research, since the bandwidth of its ultra-narrow transmission band is compatible to numerous microwave devices.

Our group has proposed and experimentally demonstrated a narrow-passband microwave photonic filter based on PM-IM conversion employing a PSFBG served as a reflection filter with an ultra-narrow notch [79].

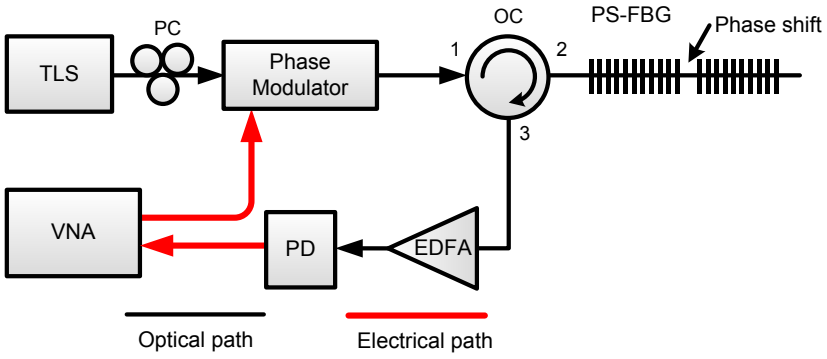

Fig. 2-6 Schematic of the PSFBG-based MPF. [79]

The schematic of the microwave photonic filter is shown in Fig. 2-6. An optical carrier is modulated by a microwave signal at a phase modulator. The phase-modulated signal, given by

$$E_{\mathrm{PM}}(t)=E_{\mathrm{1x}}\exp\left\{j\left[\omega_{\mathrm{l}}t+\pi\frac{V_{\mathrm{E}}}{V_{\pi}}\cos(\omega_{\mathrm{m}}t)\right]\right\}\approx E_{\mathrm{1x}}\sum_{n=0,\pm1}(-1)^{n}J_{n}(\beta)\exp\left[j(\omega_{\mathrm{l}}t+n\omega_{\mathrm{m}}t)\right] \quad (2\text{-}9)$$

is then sent to the PS-FBG. Both the carrier and the sidebands will be modified by the PSFBG. More specifically, only the component which can be reflected by the PSFBG can still remain in the OEO loop. For the frequencies, whose +1st and -1st order sideband are both reflected, as shown in Fig. 2-7, their beat notes with the carrier completely cancel each other. No microwave signal will be generated for those frequencies due to the phase difference between the -1st and +1st order sideband.

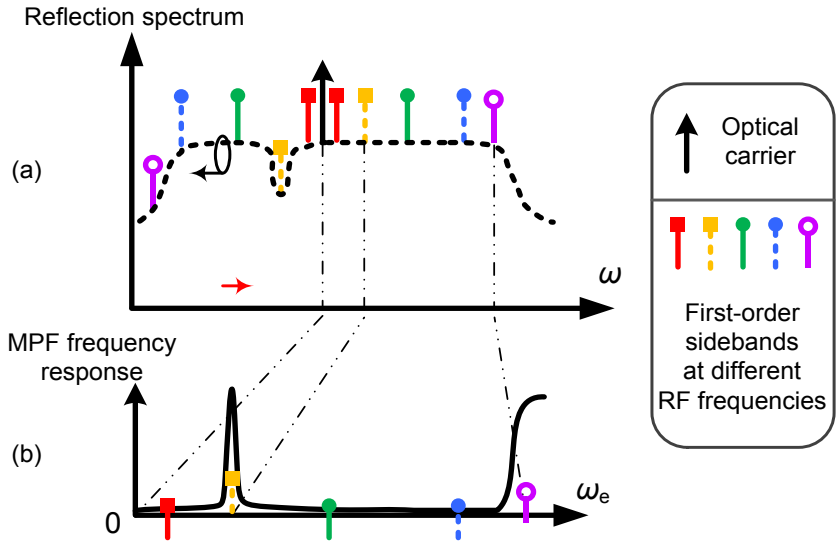

Fig. 2-7 Illustration of the operation of the MPF. (a) The reflection spectrum of the PS-FBG. (b) The frequency response of the MPF. [79]

When the modulation frequency is equal to the spacing between the carrier and the transmission notch, the corresponding first-order sideband falls in the notch of the PS-FBG, shown in Fig. 2-7, and the signal is given by Eq. (2-10).

$$E_{\mathrm{PM}}(t) \approx E_{1\mathrm{x}} + J_0(\beta)\exp\left[j(\omega_1 t)\right] + J_1(\beta)\exp\left[j(\omega_1 t + \omega_m t + \pi/2)\right] \qquad (2\text{-}10)$$

The phase-modulated signal is thus converted to an intensity-modulated signal, and envelop detection at a photodetector (PD) would lead to the generation of an electrical signal. Due to the ultra-narrow notch of the PS-FBG, a microwave photonic filter with an ultra-narrow passband is implemented.

Since the transmitted microwave signals are regenerated from the beat between the optical carrier and its sideband modified by the PSFBG, the central frequency of the passband can be tuned by either changing the wavelength of the carrier or the resonance frequency of the PSFBG. The measured frequency response of the equivalent microwave photonic filter is shown in Fig. 2-8 and the tunable frequency range is demonstrated up to 15 GHz.

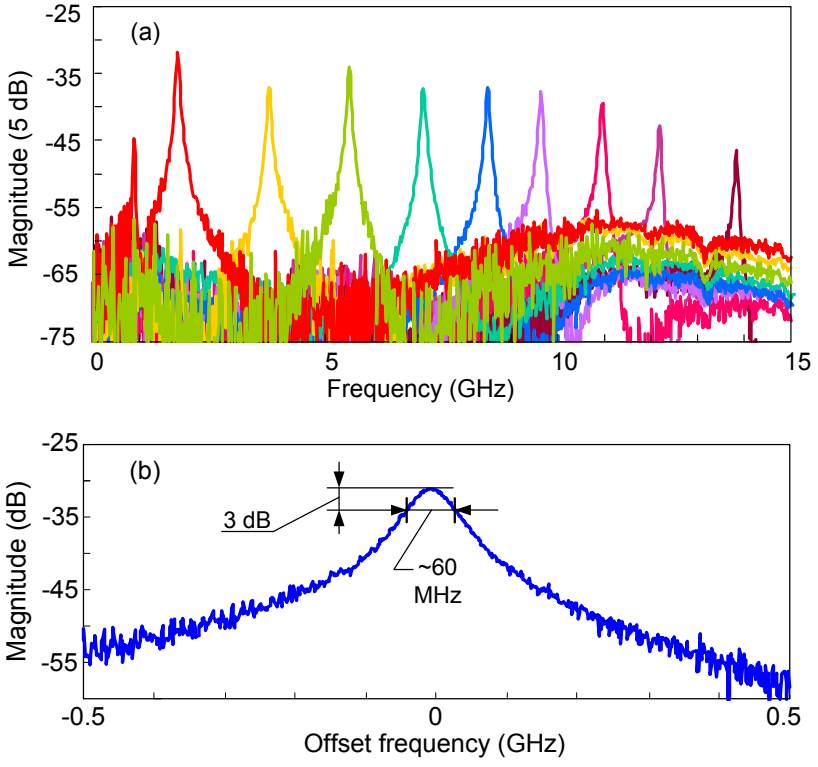

Fig. 2-8(a) Measured frequency responses of the tunable MPF (b) The zoom-in view of the frequency response when the center frequency is tuned at 6.9 GHz. [79]

Taking advantage of the narrow passband of the equivalent microwave photonic filter, which has the potential to select the condensed longitudinal mode in a long fiber loop resonator, the aforementioned technique has been applied to replace the conventional electrical filter in an OEO structure. The filtering happened in the optical domain provides larger bandwidth with even broader tunability, which is essential to the application in high speed communication system and radars. On the other hand, when the external disturbance induces structural distortion to the PSFBG, the shift of the microwave frequency carries the information of the disturbance and reveals the external environmental change. Such application in sensing is also an intensively investigated area for FBG research. Our group has demonstrated a strain sensor implemented with a microwave photonic filter-based OEO.

2.2.3 FBG senor and interrogation

The basic principle of operation used in an FBG-based sensor system is to monitor the wavelength shift of the reflected "Bragg" signal, in which the changes in the measurements (e.g., strain, temperature) are encoded. According to Eq. (2-8), both the period of the grating and the effective refractive index will determine the Bragg wavelength of the FBG: Most straightforwardly, the changes of the temperature or the axial strain will alter the period of the grating, which has been utilized to manufacture strain or temperature sensors; Alternatively, any external disturbance effect on the effective refractive index will leads to the shift of the Bragg wavelength. For example, different cladding material will result in a shifted refractive index for the evanescent filed, which results in the drift of the Bragg wavelength. With the development in coating and chemical plating technology, the FBG, especially the tiled FBG which can couple the backwards cladding modes with core modes,

can be employed as a refractometer, which has been developed in cell counting and antibody recognition system.

Demodulating or interrogating the sensing signal from the FBG sensors is to extract measurement information, such as strain, temperature or refractive index of the material, from the light signals coming from the sensor probe. Generally, demodulating the information in the form of a Bragg wavelength shift requires a spectrum analyzer. Several schemes have been proposed in order to analyze a particular type of the FBG sensors, including wavelength interrogating, intensity interrogation and frequency interrogation.

In some lab prototype sensing systems, optical spectrum analyzers (OSA) or resembled optical dispersive units are employed as demodulators. Fig. 2-9 shows a proposed wavelength interrogation setup based on arrayed waveguide grating (AWG). Broadband light sources are usually chosen in these schemes, which cover all the measuring range in wavelength. Dispersive elements such as prisms, gratings or dispersive fiber, here in particular AWG, are required to split components with different wavelengths in either space or time. Finally, extracting the space or time dependent signal from the detector allows one to reconstruct the optical reflected spectrum of the FBG and obtain the Bragg wavelength.

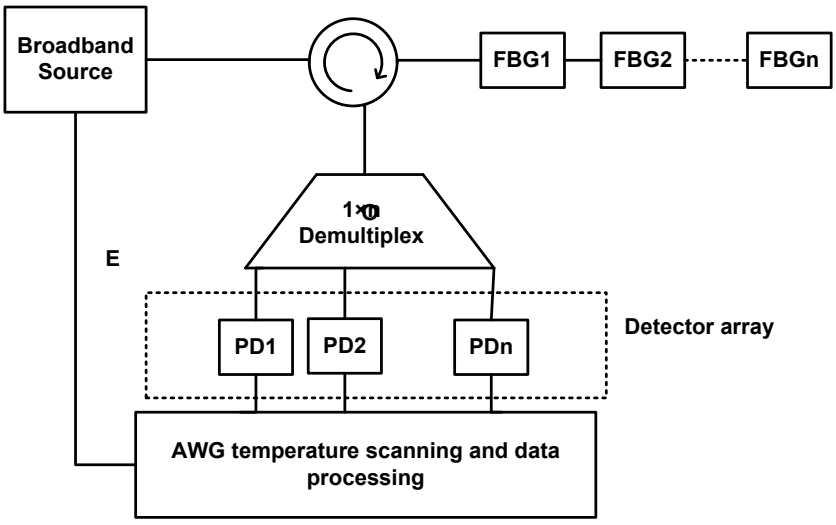

Fig. 2-9 Setup for the wavelength interrogation of distributed FBG sensors by an AWG-based demultiplexer. PD1, PD2, PDn are detectors. [80]

The optical spectrum analyzers (OSA) are not preferable in some real FBG sensor systems. The wavelength scanning mechanism usually limits its speed and accuracy.

Instead of reconstructing the whole spectrum, the signal can also be characterized by the shape of the spectrum, in particular, the slope or the edge. When light goes through a FBG, the grating can be considered as an optical filter which modified both the amplitude and the phase of an optical signal. If the Bragg wavelength shifts, the modification to a certain wavelength will also change accordingly. As long as the relation between the spectrum shift and the changes in modification is resolved, we can indirectly demodulate the sensing signal with only one or a few discrete wavelengths.

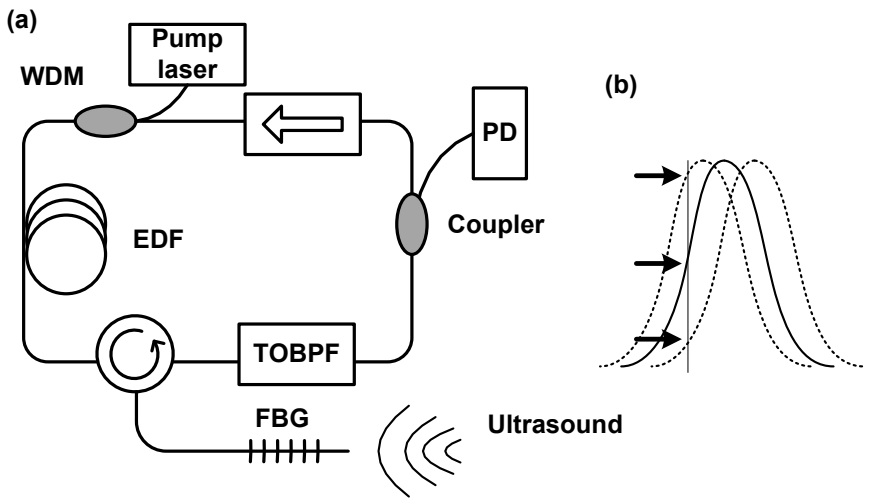

Fig. 2-10 Schematic of (a) the proposed FBG based laser ultrasonic sensor system; (b) the reflection spectrum of the sensing FBG and the effect of the ultrasonic signal on the spectrum; and (c) the transmission spectrum of the tunable band pass filter. [81]

Fig. 2-10(a) shows a laser ultrasonic sensor system interrogated with intensity demodulation scheme. The ultrasound signal acts on the FBG and jiggles its reflection spectrum. The reflectivity variations depend on the intensity ultrasound with the same frequency, as shown in Fig. 2-10(b). The lasing wavelength is set on the edge of the FBG reflection band, therefore by monitoring the intensity of the laser output, the intensity and the frequency of ultrasound signal can be demodulated from the FBG-based transducer.

Even though the intensity demodulation possess numerous advantages, such as fast speed and low-cost setup, the limitations of the intensity demodulation are still obvious. Comparing to frequency or the wavelength of a signal, the intensity is relatively easy to be disturbed by instabilities of the sensor system itself; for instance, the coupling efficiency of the connectors and even the losses in the waveguide can degrade the accuracy.

In order to keep both fast interrogation speed and high accuracy, a frequency interrogation technique is proposed incorporating optical heterodyning and microwave frequency detection.

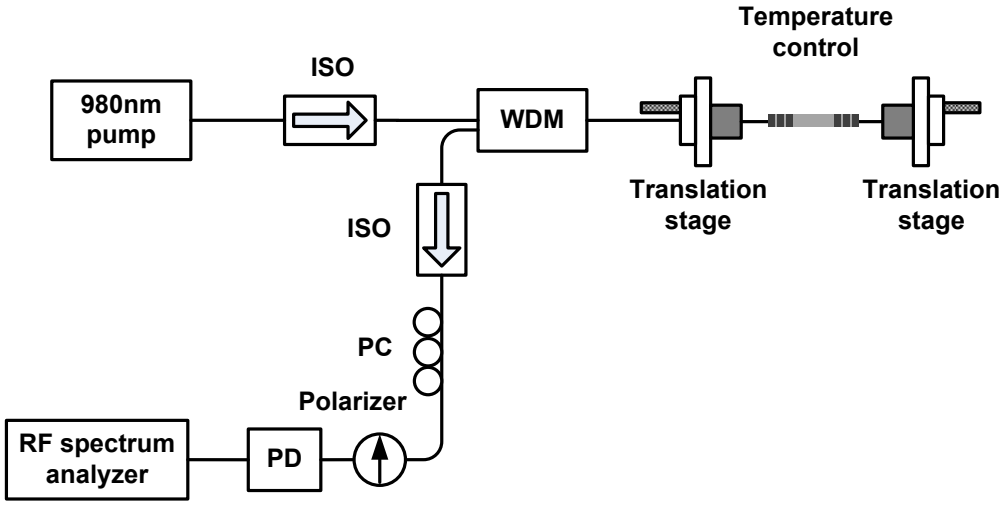

Fig. 2-11 Experimental setup of the proposed sensor[82]. PD: Photodetector. WDM: Wavelength division multiplexer. PC: Polarization controller. ISO: Isolator.

Fig. 2-11 shows the experimental setup for strain-insensitive temperature sensing [82]. The employed active fiber is a polarization maintaining Er-doped fiber with a core ellipticity of 97.5 %. The laser itself served as both source and a sensor. Since the fiber is birefringent, two lasing wavelength can be generated along two principal axes of the DFB laser. The beat note of these two wavelengths is associated with the spacing between them. By detecting the beat frequency, sensing information in the optical signal is down converted into a microwave signal. Thanks to the mature and low cost frequency detection and analysis techniques, the signal interrogation is relatively easy to achieve. Generally, the variation which changes the birefringence can be encoded in to such sensor scheme, such as temperature, bending, twisting and transverse strain.

However, the instability remains a major challenge for the laser setup. The mode competition and the thermal effect of the active medium will induce variation to the

inversed population and will further change the threshold condition to each lasing wavelength. Thereby, the quality of the sensing signal will be degraded and can hardly produce continuous and stable beat signal output.

Chapter 3

Dual-frequency Optoelectronic Oscillator

Polarization is one of the key parameters to describe a light wave. However, to our best knowledge, among the previous research work on exploiting various types of OEOs, the investigation on its polarization property still remains blank.

In this Chapter, we implemented a dual-frequency OEO for the first time, which possesses two orthogonally polarized light waves in the OEO loop structure by using a polarization maintaining phase-shifted fiber Bragg Grating (PM-PSFBG) as mode selection unit in an OEO loop. This permits the two orthogonally polarized light waves to be supported in the OEO loop simultaneously. According to the theoretical prediction to the characteristics of the PM-PSFBG, a demonstration of a PM-PSFBG based transverse load sensor is performed experimentally, which realized frequency interrogation to PSFBG load sensor by incorporating the proposed dual-frequency OEO. The high frequency purity and stability of the generated RF signal by the OEO permit high speed and high accuracy measurement.

3.1 Principle of operation

3.1.1 OEO schematics

According to the analysis in Chapter 2, the microwave frequency filtering can be realized in either the electrical domain or in the optical domain. In Section 2.2, a PSFBG-based microwave photonic filter is presented with a bandwidth narrow enough to select a single mode in the OEO system. Therefore we used a standard OEO configuration but with a polarization dependent microwave photonic filter to achieve the multi-frequency microwave signal generation.

Fig. 3-1 shows the configuration of the proposed dual-frequency OEO incorporating a PM-PSFBG. An optical carrier from a laser source is sent to a polarization modulator (PolM) via a polarization controller (PC1). The PolM is a special phase modulator that supports phase modulation along the orthogonal principal axes with opposite modulation indices. For simplicity, here we assume that the incident light is aligned with one of the principal axis of the PolM and thus the PolM is operating as a phase modulator. The phase-modulated signal is then sent to the PS-FBG through an optical circulator (OC). One sideband of the phase-modulated signal is removed by the notch of the PSFBG, and the phase-modulated signal is converted to a single-sideband intensity-modulated (SSB-IM) signal and is detected at a photodetector (PD).

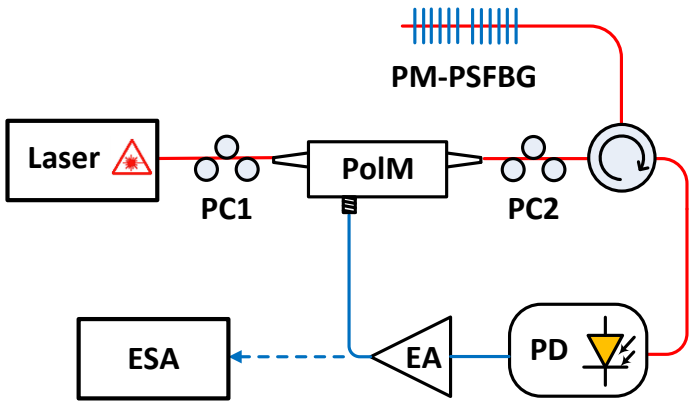

Fig. 3-1 The configuration of the proposed dual-frequency OEO. PolM: polarization modulator; PC: polarization controller; PD: photodetector; EA: electrical amplifier; ESA: electrical spectrum analyzer; PS-FBG: phase-shifted fiber Bragg grating; OC: optical circulator.

The detected electrical signal is sent back to the PolM after amplification by an electrical amplifier (EA), to close the OEO loop. Mathematically, the electrical field at the output of the PolM is given by

$$\begin{aligned} E_{\mathrm{PM}}(t) &= E_0 \exp\left\{ j\left[\omega_{\mathrm{c}} t + \pi \left(\frac{V}{V_{\pi\,\mathrm{e}}} \right) \cos\left(\omega_{\mathrm{RF}} t\right) \right] \right\} \\ &\approx E_0 \left\{ J_0(\beta) e^{j\omega_{\mathrm{c}} t} + J_1(\beta) e^{j(\omega_{\mathrm{c}}-\omega_{\mathrm{RF}})t+\pi/2} - J_1(\beta) e^{j(\omega_{\mathrm{c}}-\omega_{\mathrm{RF}})t-\pi/2} \right\} \end{aligned}, \qquad (3\text{-}1)$$

where ω_{c} is the frequency of the optical carrier, V is the voltage applied to the PolM, V_{π} is the half-wave voltage of the PolM, and ω_{RF} is the frequency of the RF signal. If we directly detect the phase-modulated signal at the PD, due to the phase difference between the +1st and -1st order sidebands, the beating between optical carrier and the +1st order sideband will completely cancel the beating between optical carrier and the -1st order sideband. However, when the phase-modulated signal is directed to the PSFBG, one sideband will be filtered out by the notch of the PSFBG and a SSB-IM signal is generated. The detection of

the SSB-IM signal at the PD will generate a RF signal. The RF signal is amplified, and then sent back to the PolM to close the OEO loop. Thus, an oscillation signal with a frequency corresponding to the spacing between the wavelengths of the optical carrier and the sideband is generated [83].

3.1.2 Birefringent PSFBG

A FBG written in single-mode fibers supports two modes simultaneously, which are orthogonally polarized. In an ideal circular-core fiber, these two modes will propagate with the same phase velocity; however, practical fibers are not perfectly circularly symmetric. As a result, the two modes propagate with different phase and group velocities.

According to the mode coupling theory [84], the electric field at a location z and at the instant t along the fiber is a linear combination of the forward and backward fields given by

$$\overrightarrow{E_{\mathrm{a}}}(x,y,z,t)=\sum_{p}A_{p}(z)\exp\lfloor i(\omega t-\beta_{p}z)\rfloor\left(\vec{e}_{p}+\vec{e}_{p}\right) \tag{3-2a}$$

and

$$\overrightarrow{E_{\mathrm{b}}}(x,y,z,t)=\sum_{q}B_{q}(z)\exp\lfloor i(\omega t+\beta_{q}z)\rfloor\left(\vec{e}_{q}+\vec{e}_{q}\right), \tag{3-2b}$$

where $\overrightarrow{E_{\mathrm{a}}}$ and $\overrightarrow{E_{\mathrm{b}}}$ are the forward and backward electric fields respectively, A_p and B_q are the complex amplitudes associated with the mode p and q; β_p and β_q are their corresponding propagation constant; $\vec{e}_{p}$ and $\vec{e}_{p}$ are the transverse and longitudinal sub-modes of the mode $LP_{l_p m_p}$, similarly $\vec{e}_{q}$ and $\vec{e}_{q}$ are the transverse and longitudinal sub-mode of the mode $LP_{l_q m_q}$.

In a single mode fiber, the LP_{01} is the most guided mode; therefore, the electric field of fundamental mode can be simplified as

$$\vec{E}(x,y,z,t) = \lfloor A(z)\exp(i\beta z) + B(z)\exp(-i\beta z) \rfloor \exp(i\omega t)\vec{e}_{0,1}(x,y). \quad (3\text{-}3)$$

The coupling of the forward and backward modes is governed by coupled-mode equation for $0 \le z \le L$:

$$\frac{dA(z)}{dz} = i\kappa_{pq} B(z)\exp\left[2i(\Delta\beta)z\right], \quad (3\text{-}4a)$$

$$\frac{dB(z)}{dz} = i\kappa_{pq}^{*} A(z)\exp\left[-2i(\Delta\beta)z\right]. \quad (3\text{-}4b)$$

Here $\Delta\beta = \beta - \beta_B$; κ_{pq} is the amplitude coupling coefficient from p mode to q mode, which results in an energy exchange. Assuming it is lossless in the grating region, therefore $\kappa_{qp} = \kappa_{pq}^{*}$. With a weak disturbance in the refractive index along the longitudinal direction, the coupling coefficient is given by

$$\begin{aligned} \kappa_{pq} &= \frac{\omega}{4}\vec{e}_q(x,y)\,dxdy \\ &= \frac{\omega}{2}\varepsilon_0 \Delta n(z) n_{eff} \iint_{core} \vec{e}_p(x,y)\vec{e}_q(x,y)\,dxdy \end{aligned} \quad (3\text{-}5)$$

We next apply the boundary conditions, indicating that forward light incident from distant, and that there is not reflection after the grating period, that is $A(0)=1$, $B(L)=0$, a closed-form transfer matrix of a uniform FBG can then be obtained:

$$F_{uni}^{B}=\begin{bmatrix}\cosh\left(L\gamma_B\right)-\dfrac{i\Delta\beta}{\gamma_B}\sinh\left(\gamma_B L\right) & \dfrac{-i\kappa}{\gamma_B}\sinh\left(\gamma_B L\right)\\ i\dfrac{\kappa}{\gamma_B}\sin\gamma_B L & \cosh\left(L\gamma_B\right)+\dfrac{i\Delta\beta}{\gamma_B}\sinh\left(\gamma_B L\right)\end{bmatrix}, \tag{3-6}$$

where $\gamma_B=\sqrt{\kappa^2-\left(\Delta\beta\right)^2}$ and L is the length of the uniform section.

The PSFBG can be considered as two pieces of uniform FBG connected by a phase shifting section which can be represented by a 2 by 2 transfer matrix given by Eq. (3-7):

$$F_{\mathrm{ps}}^{B}=\begin{bmatrix}\exp\left(-i\dfrac{2\pi n_{\mathrm{eff}}}{\lambda}\Delta z\right) & 0\\ 0 & \exp\left(i\dfrac{2\pi n_{\mathrm{eff}}}{\lambda}\Delta z\right)\end{bmatrix} \tag{3-7}$$

where *Δz* is the separation of the two uniform grating sections.

Therefore the transfer function of the PSFBG is given by the relation showing in Eq (3-8)

$$F=F_{\mathrm{uni}}^{B}F_{\mathrm{ps}}^{B}F_{\mathrm{uni}}^{B} \tag{3-8}$$

And the reflectivity can be exacted by the relation $R=\left|-\dfrac{F(2,1)}{F(2,2)}\right|^2$, where $F(2,1)$ and $F(2,2)$ are the elements in the 2 × 2 F matrix.

To resolve the transmission or the reflection spectrum of an FBG, the effective refractive index needs to be determined first. In optics the refractive index or index of refraction *n* of a substance (optical medium) is a dimensionless number that describes how light, or any other radiation, interacts with the atomic system. When light propagates

through the medium, the electrons of the atomic system are driven by the varying potential of the electric field created by incident beam. The outer electron and the ion form a dipole oscillating with the same frequency as that of the incident light. Then this oscillation will re-radiate the energy by emitting a same photon and the light continue to propagate through the medium. For different atomic systems, or different materials, the response time of this process or the relative speed at which electrical signals travel through a material varies with the type of signal and its interaction with the electronic structure, and is determined by the dielectric constant of the material. Macroscopically, the relative speed propagating in substance to that in vacuum describes such property, which is defined as the refractive index n.

In some materials the refractive index depends on the polarization and propagation direction of the light. This is called birefringence or optical anisotropy. The term anisotropy refers to a non-uniform spatial distribution of properties, which results in different values of the refractive index being obtained. Birefringence is formally defined as the double refraction of light in a transparent, molecularly ordered material, which is manifested by the existence of orientation-dependent differences in refractive index.

If the PSFBG is written on a birefringent fiber, the coupling can happen between two polarized modes. In the case of highly birefringent (Hi-Bi) fibers, the propagation constants of the two orthogonally polarized modes are made quite different from each other so that the coupling between the two modes is greatly reduced. Thus, if the light is coupled to only one of the polarized modes, most of the light remains in the same polarized mode. Therefore the total reflection can be considered as a linear combination of those from both polarization states. Assuming that a linear polarized light, with an angle θ to one of the principal axis, incident into the PM-PSFBG, the reflection spectrum can be described by

$$R(\lambda) = \cos^2\theta R\left(\lambda, n_{eff,fast}\right) + \sin^2\theta R\left(\lambda, n_{eff,slow}\right), \tag{3-9}$$

where R_{fast} and R_{slow} are the reflection spectrums along fast and slow axes, respectively; and $n_{\text{eff,fast}}$ and $n_{\text{eff,slow}}$ are the effective refractive index corresponding to principal axes. The polarization dependence is plotted in Fig. 3-2 with angles of 0, $\pi/8$, and $\pi/4$.

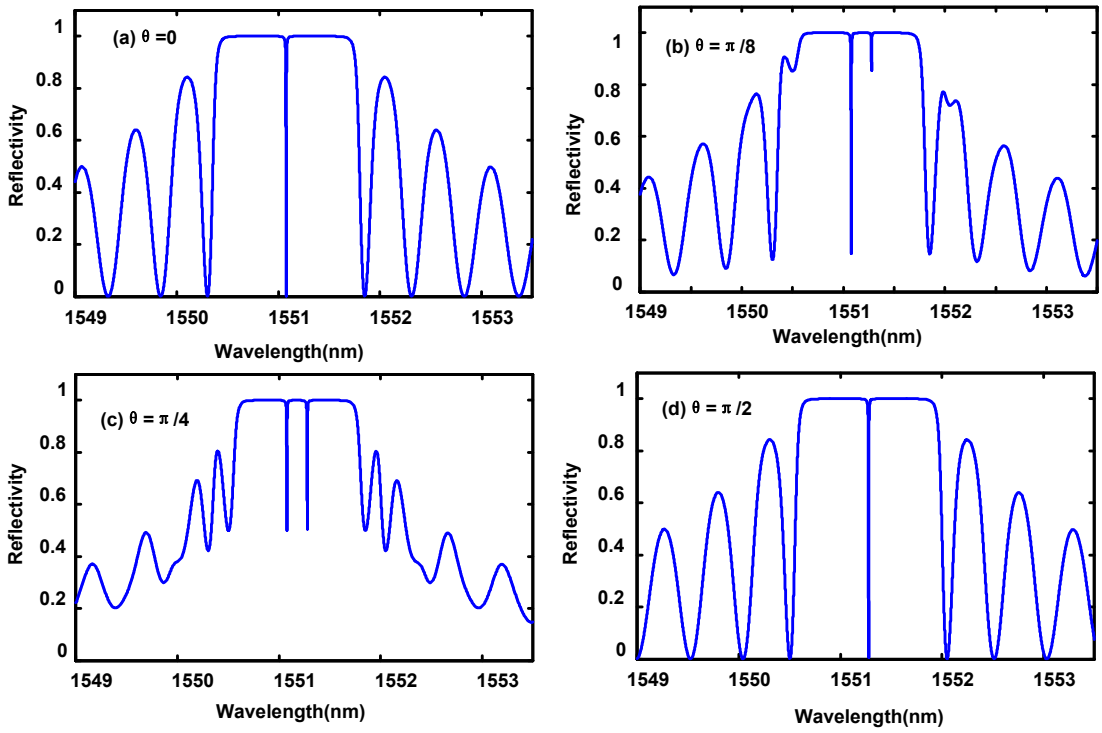

Fig. 3-2 The simulated reflection spectra of PM-PSFBG with different incident angle. (a) θ=0; (b) θ=π/8; (c) θ=π/4; (d) θ=π/2

As can be seen from Fig. 3-2, when the electric field is aligned with the fast axis, the PM-PSFBG will have the same reflection spectrum as an ordinary PSFBG. According to the statement in Eq. (3-1), this will leads to only one microwave signal to be generated. However, when the incident light is along neither fast nor slow axis of the FBG, multiple notches will appears due to the fiber birefringence. Each of the notches forms a microwave

photonic filter corresponding to one of the polarization state, shown in Fig. 3-3. The frequencies of the two passband will be determined by the spacing between the optical carrier and the two notches. Therefore, multiple-frequency microwave signals can be produced.

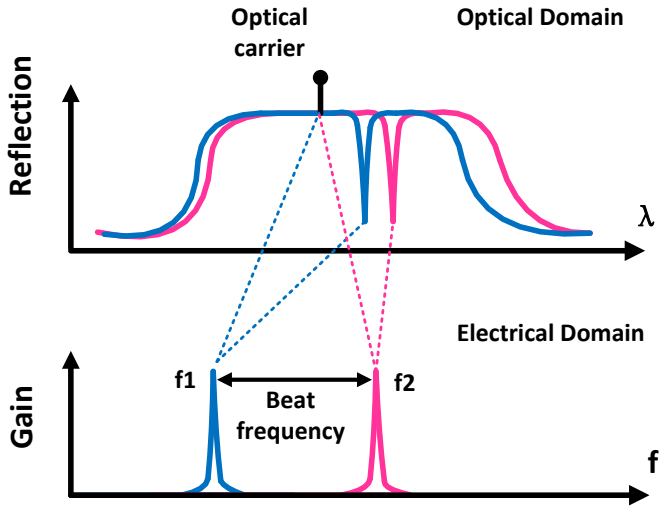

Fig. 3-3 The mechanisms to form a dual pass band microwave photonic filter with a PM-PSFBG.

3.1.3 Externally induced refractive index change

When the FBG is subjected to an external disturbance *P*, for instance, the static or dynamic strain, pressure, bending or micro-bending, the Bragg wavelength will shift accordingly [85]. The change is given by

$$d\lambda_B = 2\left[\Lambda\left(\frac{\partial n_{eff}}{\partial P}\right)_{dT=0} + n_{eff}\left(\frac{\partial \Lambda}{\partial P}\right)_{dT=0}\right]dP + 2\left[\Lambda\left(\frac{\partial n_{eff}}{\partial T}\right)_{dP=0} + n_{eff}\left(\frac{\partial \Lambda}{\partial T}\right)_{dP=0}\right]dT \quad (3\text{-}10)$$

Waxler and Cleek have studied the temperature and pressure effects on the refractive index of some oxide glasses including fused silica. They reported that the refractive index changes of the fused silica due to temperature changes are much smaller than changes due to volume variation [86]. The temperature sensitivity of FBG depends on the type of coating material and could be either increased or decreased by choosing a specific coating material for the grating zone. Under a constant temperature, the shift of Bragg wavelength only responds to the variation of the external pressure effects and the second temperature dependent term on the right side is eliminated.

Strain-induced birefringence arises because of changes in interatomic dimensions and distortion of the outer electrons around the ions. Macroscopically, this non-isotropic load induced deformation and refractive index changes are usually described by photoelastic phenomena. The effective refractive index changes due to the photoelastic effects, by using Nye's notion [87], are given by

$$\Delta\left(\frac{1}{n_i^2}\right) = p_{ij}\varepsilon_j \quad (i,j = 1,2,3,4,5,6)\,, \tag{3-11}$$

where p_{ij} is photoelastic tensor. In a Cartesian coordinate system an isotropic material photoelastic tensor is given by

$$p_{mn}=\begin{bmatrix} p_{11} & p_{12} & p_{13} & 0 & 0 & 0 \\ p_{12} & p_{11} & p_{12} & 0 & 0 & 0 \\ p_{12} & p_{12} & p_{11} & 0 & 0 & 0 \\ 0 & 0 & 0 & \dfrac{(p_{11}-p_{12})}{2} & 0 & 0 \\ 0 & 0 & 0 & 0 & \dfrac{(p_{11}-p_{12})}{2} & 0 \\ 0 & 0 & 0 & 0 & 0 & \dfrac{(p_{11}-p_{12})}{2} \end{bmatrix}, \tag{3-12}$$

And the strain tensor ε_j is given by a 6×1 column vector. Therefore, the refractive index changes in Eq. (3-11), developed to the first order, are given by

$$\Delta\left(\frac{1}{n_1^2}\right)=-2\frac{\Delta n_1}{n_1^3}=p_{11}\varepsilon_1+p_{12}\left(\varepsilon_2+\varepsilon_3\right), \tag{3-13a}$$

$$\Delta\left(\frac{1}{n_2^2}\right)=-2\frac{\Delta n_2}{n_2^3}=p_{11}\varepsilon_2+p_{12}\left(\varepsilon_1+\varepsilon_3\right), \tag{3-13b}$$

$$\Delta\left(\frac{1}{n_3^2}\right)=-2\frac{\Delta n_3}{n_3^3}=p_{11}\varepsilon_3+p_{12}\left(\varepsilon_1+\varepsilon_2\right), \tag{3-13c}$$

$$\Delta\left(\frac{1}{n_4^2}\right)=-2\frac{\Delta n_4}{n_4^3}=\frac{\left(p_{11}-p_{12}\right)}{2}\varepsilon_4, \tag{3-13d}$$

$$\Delta\left(\frac{1}{n_5^2}\right)=-2\frac{\Delta n_5}{n_5^3}=\frac{\left(p_{11}-p_{12}\right)}{2}\varepsilon_5, \tag{3-13e}$$

$$\Delta\left(\frac{1}{n_6^2}\right)=-2\frac{\Delta n_6}{n_6^3}=\frac{\left(p_{11}-p_{12}\right)}{2}\varepsilon_6, \tag{3-13f}$$

Assuming that only normal stress is posed onto the material, all terms associated with the shear stress, ε_4, ε_5, ε_6, will be eliminated. By applying the stress strain relation:

$$\varepsilon_1 = \frac{1}{E}\left[\sigma_1 - \nu\left(\sigma_2 + \sigma_3\right)\right], \tag{3-14a}$$

$$\varepsilon_2 = \frac{1}{E}\left[\sigma_2 - \nu\left(\sigma_1 + \sigma_3\right)\right], \tag{3-14b}$$

$$\varepsilon_3 = \frac{1}{E}\left[\sigma_3 - \nu\left(\sigma_1 + \sigma_2\right)\right], \tag{3-14c}$$

the refractive index changes along the principle axes in a fiber system can be derived from (3-13a) and (3-13b):

$$\Delta n_1 = -\frac{n_1^3}{2E}\left\{\left(p_{11} - 2\nu p_{12}\right)\sigma_1 + \left[\left(1-\nu\right)p_{12} - \nu p_{11}\right]\left[\sigma_2 + \sigma_3\right]\right\}, \tag{3-15a}$$

$$\Delta n_2 = -\frac{n_2^3}{2E}\left\{\left(p_{11} - 2\nu p_{12}\right)\sigma_2 + \left[\left(1-\nu\right)p_{12} - \nu p_{11}\right]\left[\sigma_1 + \sigma_3\right]\right\}. \tag{3-15b}$$

The separation between the two Bragg wavelengths in a PM-PSFBG according to Eq. (3-10) is given by

$$\Delta\lambda_B = 2\Lambda\left(\Delta n_1 - \Delta n_2\right) = -\frac{n_0^3\Lambda\left(1+\nu\right)\left(p_{11} - p_{12}\right)}{E}\left(\sigma_1 - \sigma_2\right). \tag{3-16}$$

As can be seen from the Eq. (3-16), the spacing between the two Bragg wavelengths, or the two ultra-narrow transmission bands in PM-PSFBG, responds linearly to the transverse strain applied to it. Therefore, the strain information can be demodulated from the reflection spectrum of the PM-PSFBG.

The separation between the two reflection notches can also be resolved from the electrical domain instead of optically. The beat note generated from the dual-frequency

optoelectronic oscillator is associated to the spacing between the two oscillating modes. If a transverse force is applied to the PS-FBG, the birefringence of the fiber will be changed. The notch will then be split into two notches due to different refractive indices along the orthogonal directions. According to the of Hertz theory of contact force and strain relation [88, 89], the changes in the frequency spacing between two notches along the two orthogonal polarization states is given by the

$$\Delta\omega = \omega_x - \omega_y = \frac{2cn_0^2\left(p_{11} - p_{12}\right)\left(1+\nu_p\right)\cos\left(2\theta\right)F}{\pi r E \lambda_0}, \tag{3-17}$$

where and p_{11} and p_{12} are the components of the strain-optical tensor of the optical material, ν_p is Poisson's ratio, E is the Young's modulus of the fiber, r is the radius of the fiber, θ is the angle between the direction of the force and the polarization axis of the fiber, and F is the linear transverse load (force per unit length).

Due to the load-interrelated notches along the orthogonal polarization directions, two RF signals at different frequencies are generated by the OEO. The beating between the two RF signals will generate a third microwave signal with its frequency being a function of the load-induced birefringence. Thus, by measuring the beat frequency, the transverse load applied to the PS-FBG can be measured. By using the typical values of a silica fiber at a wavelength of 1550: n_0 = 1.467, p_{11} = 0.12, p_{12} = 0.27, ν_p = 0.17, E = 7.6×10^4 N/mm and the radius of optical fiber r = 62.5 μm, we have the ratio between the transverse load the beat frequency given by 9.6 GHz/(N/mm).

3.2 Experiment

3.2.1 Dual-frequency OEO experiment

A proof-of-concept experiment to demonstrate the stable operation of the proposed OEO is performed. A PSFBG written in a polarization maintaining fiber is fabricated. Due to the intrinsic birefringence, two notches with an initial notch separation of 6.02 GHz are produced. The 3-dB bandwidth of each of the notches is ~30 MHz, which is narrow enough to ensure only a single longitudinal mode oscillation inside the OEO loop for each polarization state.

When a linearly polarized incident light with an angle of 45^{o} relative to one principal axis of the PolM is sent to the PolM, the light is equally projected to the two orthogonal polarization axes; thus, a photonic microwave filter having dual passbands with a band separation of 6.02 GHz is generated. Fig. 3-4(a) shows the passband of the filter along the horizontal or vertical polarization direction, measured by aligning the incident light having an angle of 0^{o} or 90^{o} relative to one principal axis of the PolM. Fig. 3-4(b) shows the filter response when the incident light is aligned with an angle of 45^{o} relative to one principal axis of the PolM. A dual pass band filter is realized.

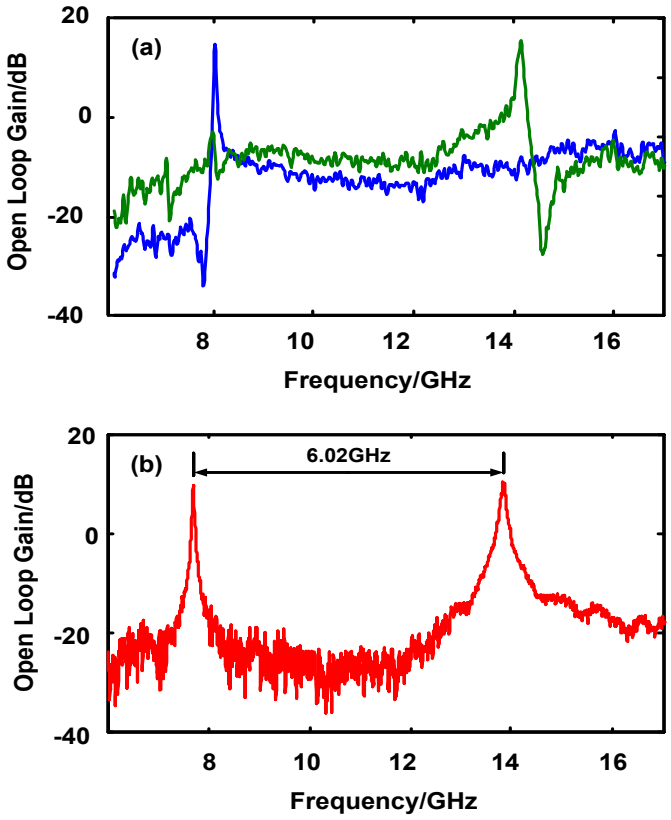

Fig.3-4 (a) Single passband photonic microwave filter when the incident light is alighted with an angle of 0^o or 90^o relative to one principal axis of the PolM. (b) Dual passband photonic microwave filter when the incident light is alighted with an angle of 45° relative to one principal axis of the PolM.

Based on the analysis in Section 2.1, when the OEO loop is closed and the gain for both the two frequencies can compensate their loss along the loop; in other words, the small signal gain goes above 0 dB; two microwave signals at two frequencies determined by center frequencies of the two passbands will be generated. Due to the intrinsic birefringence of the PSFBG, two microwave signals, shown in Fig. 3-5(a) noted as ω_x , ω_y , are generated at 8.22 GHz and 14.24 GHz, respectively. Note that due to the nonlinearity of the PD, a third signal that is the beat note of the two microwave signals is also generated at 6.02 GHz.

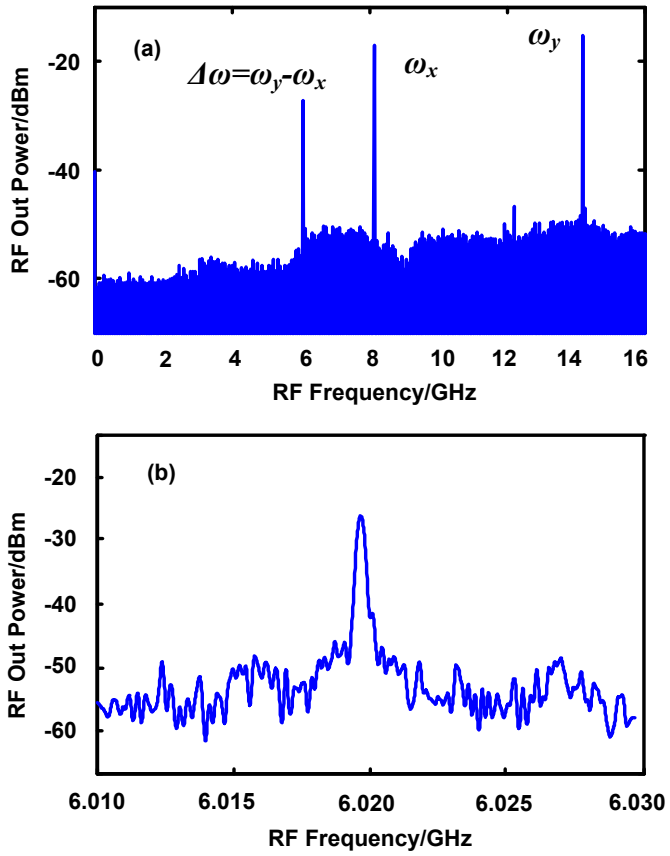

Fig. 3-5 (a) The electrical spectrum of the signal generated by the dual-frequency OEO, with two microwave signals at 8.22 GHz and 14.24 GHz and a beat signal at 6.02 GHz. (b) the zoom-in view of the beat signal.

3.2.2 Transverse load sensing experiment

An experiment of the proposed sensor is also performed with a planar transverse load subject to the PM-PSFBG. To ensure the system reaches its highest sensitivity and to have a good linearity between the transverse load and the beat frequency, in the experiment the transverse load is applied to the PS-FBG along the fast axis. Note that a supporting fiber with an identical radius is placed in parallel with the PSFBG to ensure the load is transversely applied. By increasing the load applied to the PSFBG, the beat frequency is shifted linearly towards a smaller frequency, as shown in Fig. 3-6(b). The spectrum of the

beat signal is measured by an ESA (Agilent E4448A), with the spectrum shown Fig. 3-6 (c). The slope through linear fitting is -9.73 GHz/ (N/mm) which agrees well with the theoretical value of 9.6 GHz/ (N/mm).

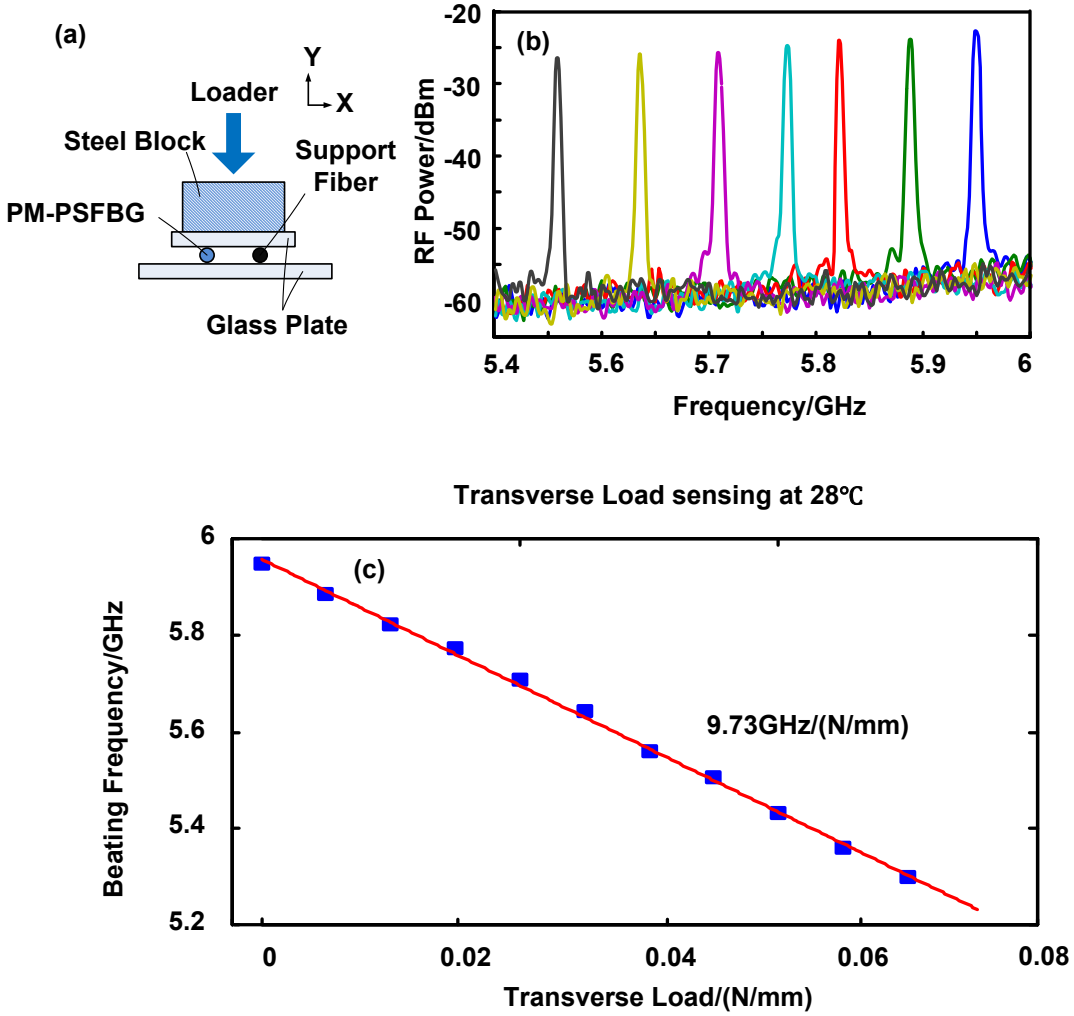

Fig.3-6 (a) The implementation of the planar strain on transverse direction. (b) The electrical spectrum with different load. (c) Measured beating frequency as a function of applied transverse load and the electrical spectrum with different load.

The stability of the sensor system is then studied. To do so, we let the system to operate in a room environment for two hours. The variation of the beating frequency is within 1 MHz. The resolution of the proposed sensor system is also studied. The resolution

is limited by its free spectrum range (FSR). In this system the FSR is calculated to be about 2 MHz, which corresponds to a resolution of 2.06×10^{-4} N/mm. As a high Q optical filter, the PSFBG guaranteed the single mode operation of OEO when the gain in the loop is properly controlled. More importantly, the mode hopping is not observed in our experiment.

The impact of the temperature change to the measurement is also studied. Although the birefringence of the fiber will be affected by temperature variation, such effect is much less significant than the birefringence induced by the geometrical asymmetry due to the transverse load. It is demonstrated that the change in the beat frequency is within 2 MHz when the temperature is increased from 28 to 48^{o}C.

In the experiment, the PS-FBG is fabricated using a polarization maintaining fiber, which ensures an initial birefringence, leading to a non-zero beat frequency at ~6 GHz. The PS-FBG can be replaced by a regular PSFBG written in a single-mode fiber without initial birefringence. Thus, the beating frequency can be lower. The benefits of a system operating at a low interrogation frequency are obvious: the interrogation system can be implemented using lower frequency components at a lower cost.

We should note that the accuracy of the sensor is not affected by the wavelength drift of the laser source since the impact of wavelength drift is eliminated by the simultaneous shifting of the two oscillating frequencies. This property is important and can reduce significantly the system cost since no precise control over the wavelength of the laser source is needed. However, the two oscillating frequencies still depend on the carrier wavelength, which eventually limits the measurement range of the sensor.

3.3 Summary

To summarize this section, we have proposed and experimentally demonstrated a dual-frequency OEO incorporating a PM-PSFBG with two oscillating microwave frequencies. The non-harmonic frequencies, including one beat note, can be support simultaneously in an OEO setup. The two oscillating frequencies were determined by the spacing between the optical carrier and the two notches. Based on the nonlinearity of the PD and the generated beat note, a high resolution and fast-speed interrogated fiber optic transverse load sensor was implemented. The fundamental concept of the work was the use of an OEO incorporating a PM-PSFBG to which a transverse load was applied, to translate the force applied to the PM-PSFBG to the change of the beat frequency. Since the interrogation is performed in the electrical domain, the system was simplified with an increased interrogation speed and accuracy. The proposed system was experimentally demonstrated. The sensitivity was measured to be as high as 9.73 GHz/(N/mm). The stability of the system and the independence of the system on the environmental temperature change and the wavelength drift were also studied.

Chapter 4

Dual Wavelength Fiber Ring Laser Coupled Dual-frequency OEO

Unlike the optical amplification, in which strong homogenous line broadening would increase the wavelength competition, electrical amplification has no such effect, and the stability of the dual-frequency OEO is significantly improved. The major limitation of the OEO-based approach is the possible frequency measurement ambiguity. The frequency of the beat note is not always the lowest frequency, thus it is critical to identify correctly the beat frequency to make a correct measurement.

In this chapter, we propose a dual-wavelength fiber ring laser coupled dual-frequency OEO, to generate a stable microwave signal. By encoding the sensing information in the microwave frequency, the dual-wavelength fiber ring laser coupled dual-frequency OEO can be employed as a transverse load sensor. Since only a single microwave frequency is generated, the ambiguity problem in the OEO-based approach in Chapter 3 is avoided.

The proposed fiber-optic sensor has two mutually coupled loops: the fiber ring loop and the OEO loop. A polarization-maintaining phased-shifted fiber Bragg grating (PM-PSFBG) is incorporated in the two loops. In the fiber ring loop, the use of the PM-PSFBG would generate two optical wavelengths with the wavelength spacing determined by the birefringence of the polarization-maintaining fiber (PMF). In the OEO loop, a microwave signal with its frequency also determined by the birefringence of the PMF is generated, which is fed back into the fiber ring loop to injection-lock the dual wavelengths. Due to the injection locking, a very stable dual-wavelength operation is reached. The beating between

the dual wavelengths generates a microwave signal which is used to implement high-speed and high-resolution transverse load sensing. The high spectrum purity and high stability of the generated microwave signal permits high accuracy and always valid measurement, and the time-domain frequency measurement allows the interrogation at an ultra-high speed. An experiment is performed. A dual-wavelength fiber ring laser with an ultra-stable operation is demonstrated. The use of the fiber ring laser to perform transverse load sensing is also demonstrated. A sensitivity as high as +9.757 GHz/(N/mm) and -9.735 GHz/(N/mm), along the fast and slow axes, respectively, is realized.

4.1 Principle of operation

4.1.1 Fiber ring laser coupled OEO structure

The schematic diagram of the fiber ring laser coupled OEO is shown in Fig. 4-1. As can be seen from the figure the fiber ring laser coupled OEO consists of two mutually coupled loops: the fiber ring loop and the OEO loop. A path consisting of a phase modulator (PM) and a PM-PSFBG are shared by the two loops. For the fiber ring loop, the lasing is established due to the gain of the erbium-doped fiber amplifier (EDFA). The dual wavelength selection is realized due to the dual passbands of the PM-PSFBG along the two principal axes. For the OEO, the oscillation is started due to the gain from the electrical amplifier (EA). The oscillation frequency is determined by the central frequency of an equivalent microwave filter formed due to the PM-IM conversion in the PM-PSFBG. The generated microwave signal is re-injected into the fiber ring cavity at the PM, which is the key to improve the stability of the fiber ring laser.

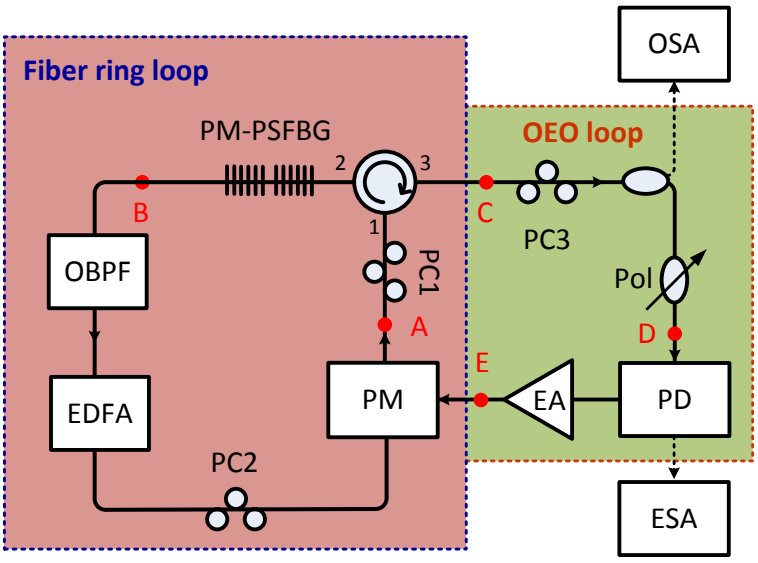

Fig. 4-1. The schematic of the proposed fiber ring laser coupled OEO. PM: phase modulator; PC: polarization controller; PD: photodetector; EA: electrical amplifier; PM-PSFBG: polarization

maintaining phase-shifted fiber Bragg grating; OBPF: optical bandpass filter; Pol: polarizer; OSA: optical spectrum analyzer; ESA: electrical spectrum analyzer; EDFA: erbium-doped fiber amplifier.

4.1.2 Fiber ring loop

The fiber ring loop consists of an EDFA, a PM-PSFBG serving as a dual-wavelength optical bandpass filter, an optical bandpass filter (OBPF), a PM, and two polarization controllers (PC1 and PC2). In the system, the PM supports phase modulation only along one polarization direction.

The PM-PSFBG is the key device in the fiber ring loop that ensures dual wavelength operation. In fact, the PM-PSFBG is written in a PMF with a phase shift introduced into the grating during the fabrication. Due to the birefringence of the PMF, the refractive indices along the two principal axes are slightly different, which leads to two ultra-narrow and slightly separated transmission bands at λ_1 and λ_2. The incorporation of the PM-PSFBG into the fiber ring loop would lead to the generation of two orthogonally polarized light waves at λ_1 and λ_2 with each operating in the single-longitudinal mode due to the ultra-narrow width of each of the transmission bands.

Assuming that the light wave at point A is the summation of two light waves with their wavelengths at λ_1 and λ_2, the complex amplitude of the electric field of the light wave can be described by a Jones vector. Since the PM supports phase modulation along only one polarization direction (x axis, the principal axis of the PM), only the components in the Jones vector along the x axis have non-zero values, E_{1x} and E_{2x}, which are the complex amplitude along principal axis of the PM corresponding to the lasing wavelengths λ_1 and λ_2. The total electric field at point A, as shown in Fig. 4-1, is given by

$$E_{\mathrm{A}} = \begin{bmatrix} E_{1\mathrm{x}} \\ 0 \end{bmatrix} + \begin{bmatrix} E_{2\mathrm{x}} \\ 0 \end{bmatrix} \tag{4-1}$$

The linearly-polarized light is sent to the PM-PSFBG through a polarization controller (PC1). The PM-PSFBG has two ultra-narrow transmission bands along the two principal axes, as shown in Fig. 4-2(a). The polarization direction of the light wave is controlled by PC1 to have an angle of θ relative to the fast axis of the PM-PSFBG, as shown in Fig. 2(b).

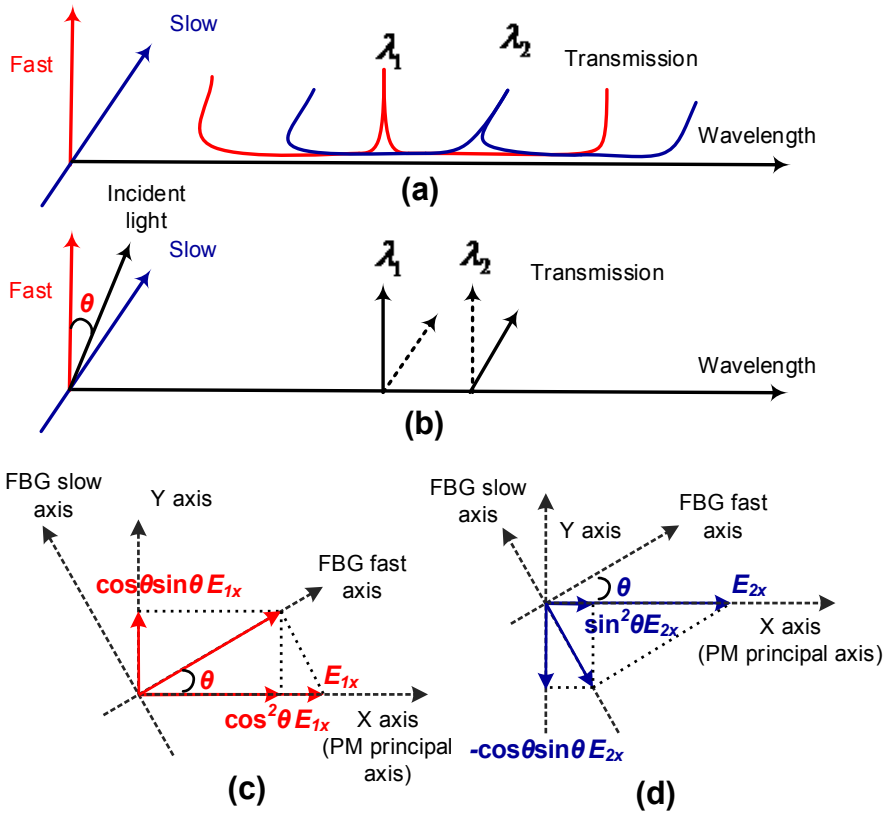

Fig. 4-2. (a) The transmission bands along the fast and slow axes of the PM-PSFBG. (b) The light waves at λ_1 and λ_2 are transmitted, respectively, along the fast and slow axes of the PM-PSFBG (solid arrows). (c) The light wave at λ_1 is transmitted through the fast axis of the PM-PSFBG and then projected to the x axis which is also the principal axis of the PM. (d) The light wave at λ_2 is transmitted through the slow axis of the PM-PSFBG and then projected to the x axis.

For the light wave at λ_1, it is incident to the PM-PSFBG with an angle of θ relative to the fast axis, thus it is split into two orthogonal components, with the one along the fast axis transmitted through the transmission band at λ_1 and the component projected to the slow axis is reflected, as shown in Fig. 4-2(c). For the light wave at λ_2, the component projected to the slow axis is transmitted through the transmission band at λ2 and the component projected to the fast axis is reflected as shown in Fig. 4-2(d). Thus, the total electric field after the PM-PSFBG at point B is given by

$$E_B = \begin{bmatrix} \cos^2(\theta) E_{1x} \\ \sin(\theta)\cos(\theta) E_{1x} \end{bmatrix} + \begin{bmatrix} \sin^2(\theta) E_{2x} \\ -\sin(\theta)\cos(\theta) E_{2x} \end{bmatrix} \tag{4-2}$$

Since the PM only supports phase modulation along the x direction, the powers of the light waves along the x direction for the two wavelengths at λ_1 and λ_2 can be adjusted by tuning the angle θ, as can be seen from Eq. (4-2). For example, when $\theta = 0$, the light wave at λ_1 will be transmitted, and the light wave at λ_2 is reflected. In this case, a single-wavelength lasing at λ_1 will be supported. When $\theta = \pi/2$, the light wave at λ_2 will be transmitted while the light wave at λ_1 is reflected. In this case, a single-wavelength lasing at λ_2 will be supported. The laser can also work in a dual-wavelength mode if the powers for the two wavelengths are balanced by tuning PC2. Due to the strong wavelength competition in the gain medium, the operation in a dual-wavelength mode is not stable. A solution to improve the stability is to introduce an OEO into the system. Through injection locking of the two wavelengths, the stability can be improved.

4.1.3 OEO loop

The OEO loop is formed by the PM-PSFBG, the PM, a polarizer (Pol), a PD, an EA, and two PCs (PC1 and PC3). The PM-PSFBG and the PM are shared with the fiber ring loop. In the OEO loop, the PM-PSFBG is operating in the reflection mode with two ultra-narrow notches along the fast and slow axes, as shown in Fig. 4-3(a). The light wave at λ_1 projected to the slow axis is reflected into the OEO loop, and the light wave at λ_2 projected to the fast axis is reflected into the OEO loop, as shown in Fig. 4-3(b).

Again, the total electric field consisting of the two reflected light waves at λ_1 and λ_2 at point C is given by

$$E_C = \begin{bmatrix} \sin^2(\theta) E_{1x} \\ -\sin(\theta)\cos(\theta) E_{1x} \end{bmatrix} + \begin{bmatrix} \cos^2(\theta) E_{2x} \\ \sin(\theta)\cos(\theta) E_{2x} \end{bmatrix} \tag{4-3}$$

The two light waves are sent to the PD through a polarizer to project the two orthogonally polarized light waves to the principal axis of the polarizer, and beat them at the PD. If the principal axis of the polarizer is oriented at an angle $\varphi = \theta - \pi/4$ relative to the principal axis of the PM, as shown in Fig. 4-3(c), we have the total electric field along the principal axis of the polarizer, given by

$$
\begin{aligned}
E_D &= \begin{bmatrix} \cos(-\varphi) & -\sin(-\varphi) \\ 0 & 0 \end{bmatrix} E_C \Big|_{\varphi=\theta-\frac{\pi}{4}} \\
&= \begin{bmatrix} \cos(-\varphi) & -\sin(-\varphi) \\ 0 & 0 \end{bmatrix} \left\{ \begin{bmatrix} \sin^2\theta E_{1x} \\ -\sin\theta\cos\theta E_{1x} \end{bmatrix} + \begin{bmatrix} \cos^2\theta E_{2x} \\ \sin\theta\cos\theta E_{2x} \end{bmatrix} \right\} \Big|_{\varphi=\theta-\frac{\pi}{4}} \\
&= \begin{bmatrix} \cos(\frac{\pi}{4}-\theta) & -\sin(\frac{\pi}{4}-\theta) \\ 0 & 0 \end{bmatrix} \left\{ \begin{bmatrix} \sin^2\theta E_{1x} \\ -\sin\theta\cos\theta E_{1x} \end{bmatrix} + \begin{bmatrix} \cos^2\theta E_{2x} \\ \sin\theta\cos\theta E_{2x} \end{bmatrix} \right\} \\
&= \begin{bmatrix} \cos(\frac{\pi}{4}-\theta)\sin^2\theta E_{1x} - \sin(\frac{\pi}{4}-\theta)\left(-\sin\theta\cos\theta\right) E_{1x} \\ 0 \end{bmatrix} \\
&\quad + \begin{bmatrix} \cos(\frac{\pi}{4}-\theta)\cos^2\theta E_{2x} - \sin(\frac{\pi}{4}-\theta)\left(\sin\theta\cos\theta\right) E_{2x} \\ 0 \end{bmatrix}.
\end{aligned}
\tag{4-4}
$$

Along the principal axis of the polarizer, it is given by

$$
\begin{aligned}
\mathrm{E}_D &= \cos(\frac{\pi}{4}-\theta)\sin^2\theta E_{1x}\cos\left(\omega_1 t\right) - \sin(\frac{\pi}{4}-\theta)\left(-\sin\theta\cos\theta\right) E_{1x}\cos\left(\omega_1 t\right) \\
&\quad + \cos(\frac{\pi}{4}-\theta)\cos^2\theta E_{2x}\cos\left(\omega_2 t\right) - \sin(\frac{\pi}{4}-\theta)\left(\sin\theta\cos\theta\right) E_{2x}\cos\left(\omega_2 t\right) \\
&= \sin\theta E_{1x}\cos\left(\omega_1 t\right)\left[\cos(\frac{\pi}{4}-\theta)\sin\theta + \cos\theta\sin(\frac{\pi}{4}-\theta)\right] \\
&\quad + \cos\theta E_{2x}\cos\left(\omega_2 t\right)\left[\cos(\frac{\pi}{4}-\theta)\cos\theta - \sin(\frac{\pi}{4}-\theta)\sin\theta\right] \\
&= \sin\theta E_{1x}\cos\left(\omega_1 t\right)\sin(\frac{\pi}{4}-\theta+\theta) + \cos\theta E_{2x}\cos\left(\omega_2 t\right)\cos(\frac{\pi}{4}-\theta+\theta) \\
&= \frac{\sqrt{2}}{2}\left[\sin\theta E_{1x}\cos\left(\omega_1 t\right) + \cos\theta E_{2x}\cos\left(\omega_2 t\right)\right],
\end{aligned}
\tag{4-5}
$$

where ω_1 and ω_2 are the angular frequencies of the light waves at λ_1 and λ_2. The photo current at the output of the PD is given by

$$i_{PD} = R\left|E_D\right|^2 = \frac{1}{4}R\sin(2\theta)E_{2x}E_{1x}\cos\left[(\omega_1-\omega_2)t\right] = I_{PD}\cos(\Omega t), \tag{4-6}$$

where R is the responsivity of the PD, $I_{PD} = \frac{1}{4}R\sin(2\theta)E_{2x}E_{1x}$ is the amplitude of the ac component and Ω is the angular frequency of the detected microwave signal. Note that in deriving Eq. (4-7), the dc component is ignored.

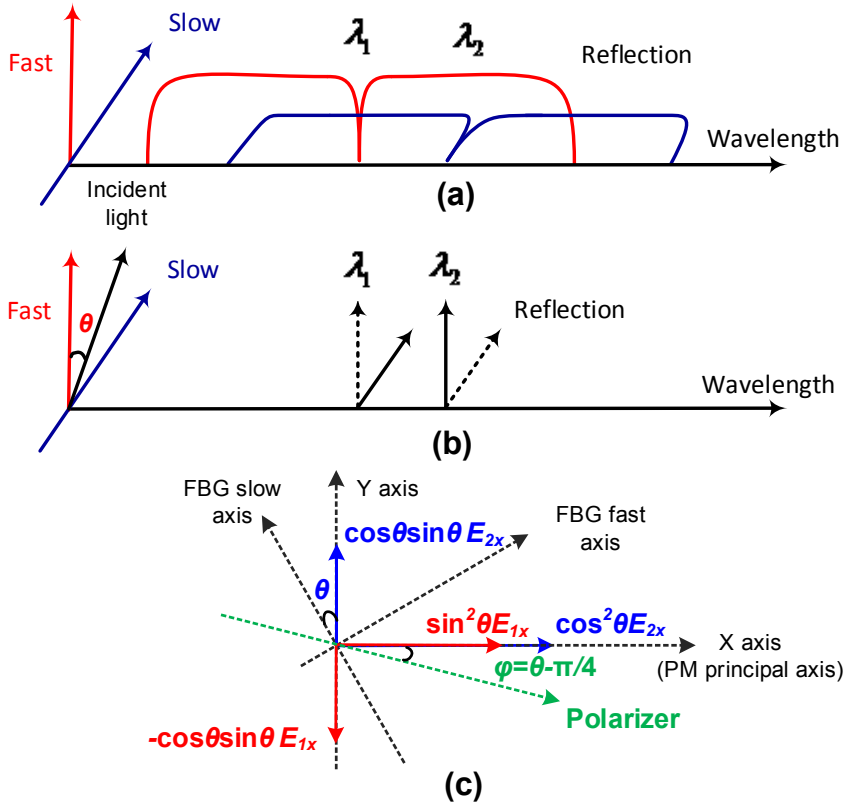

Fig. 4-3. (a) The reflection bands along the fast and slow axes of the PM-PSFBG. (b) The light waves at λ_1 and λ_2 are reflected by the PM-PSFBG, respectively, along the slow and fast axes of the PM-PSFBG. (c) The principal axis of the polarizer is oriented at an angle of $\varphi=\theta-\pi/4$ relative to the principal axis of the PM.

After amplification by an EA with a gain of G_{EA}, we have the output microwave signal at point E in Fig. 4-1. The amplitude of the microwave signal is given by

$$V_E = L_E G_{EA} Z_L I_{PD} = \frac{1}{4} L_E G_{EA} R Z_L \sin(2\theta) E_{2x} E_{1x}, \quad (4\text{-}7)$$

where L_E is the total insertion loss in the OEO loop, Z_L is the load impedance, and G_{EA} is the voltage gain of the EA.

The signal from the EA is sent back to the PM to close the OEO loop, at the same time, as an injection signal to injection lock the two wavelengths of the fiber ring laser.

4.1.4 Dual-wavelength fiber ring laser-coupled OEO

The mutual coupling between the two loops to stabilize the operation of the dual-wavelength fiber ring laser is analyzed. The dual-wavelength operation in the fiber ring laser is very unstable due to the homogenous line broadening in the gain medium which leads to strong wavelength competition. The stability can be significantly improved if an OEO loop is incorporated into the fiber ring laser.

We start our analysis by considering first only one lasing wavelength, say λ_1, as the optical carrier for the OEO, which corresponds to $\theta = 0$. When the OEO loop is closed, microwave oscillation will start. The frequency of the generated microwave signal is determined by the wavelength of the optical carrier at λ_1 and the central wavelength of the notch. Since the PM only supports phase modulation along the x direction, generally, the electric field of the phase-modulated signal at the output of the PM is given by

$$E_{\mathrm{PM}}(t) = E_{1\mathrm{x}} \exp\left\{ j\left[\omega_1 t + \pi \frac{V_{\mathrm{E}}}{V_\pi} \cos(\Omega t) \right] \right\} \approx E_{1\mathrm{x}} \sum_{n=0,\pm 1} (-1)^n J_n(\beta) \exp\left[j(\omega_1 t + n\Omega t) \right] \tag{4-8}$$

where E_{PM} is the electric field at the output of the PM (point A in Fig. 4-1) along the x direction, $E_{1\mathrm{x}}$ and ω_1 are, respectively, the electric field and the angular frequency of the optical carrier along the *x* direction, V_{E} is the voltage of the microwave signal at the output of the E_{A} (point E in Fig. 4-1), V_π is the half-wave voltage of the PM, $\beta = \pi V_{\mathrm{E}}/V_\pi$ is the modulation index, $J_{\mathrm{n}}(\beta)$ is the Bessel function of the first kind of an order *n*, and Ω is the angular frequency of the modulation microwave signal. If we directly detect the phase-modulated signal at the PD, due to out-of-phase nature of the +1st and -1st order sidebands, the beating between the optical carrier and the +1st order sideband will completely cancel the beating between optical carrier and the -1st order sideband. However, if the phase-modulated signal is directed to the PM-PSFBG, one sideband at λ_2 is filtered out and a single-sideband with carrier (SSB+C) signal is thus generated. The detection of the SSB+C signal at the PD will produce a microwave signal, which then is amplified by the EA and sent back to the PM to close the OEO loop. If the gain is greater than the total loss in the OEO loop, self-sustained oscillation will be established and a microwave signal will be generated.

If θ is adjusted such that dual-wavelength lasing is established. The stable operation of the dual wavelengths is due to the mutual injection locking. For example, for the wavelength at λ_1, the phase modulated signal has a sideband that is exactly located at the other transmission band of the PM-PSFBG at λ_2, thus the sideband at λ_2 will be injected into the fiber ring laser. Such injection provides extra energy to λ_2, which helps to initialize lasing. The two wavelengths will finally reach a steady state, due to the nonlinear effect in

both the gain medium and the PM, in which the electric field at any point of the ring loop after a round trip should keep constant. The complex amplitude after a round trip at the output of the PM (point A in Fig. 4-1) can be expressed as

$$E'_{1A} = L_O G(E_{1x}, E_{2x}) \begin{bmatrix} 1 & 0 \\ 0 & 0 \end{bmatrix} \{J_0(\beta) E_{1B} + J_{-1}(\beta) E_{2B}\}, \tag{4-9a}$$

$$E'_{2A} = L_O G(E_{1x}, E_{2x}) \begin{bmatrix} 1 & 0 \\ 0 & 0 \end{bmatrix} \{J_0(\beta) E_{2B} + J_1(\beta) E_{1B}\}, \tag{4-9b}$$

where E'_{1A}, E'_{2A}, represent the complex amplitudes for λ_1 and λ_2 at point A after a round trip, L_O is the total insertion loss in the optical fiber ring loop, $G(E_{1x},E_{2x})$ is the nonlinear gain of the optical gain medium which is a function of the input optical power. E_{1B} and E_{2B} are two 1×2 Jones vectors of the complex amplitudes at point B given in (2) for λ_1 and λ_2, respectively. The 2×2 matrix $\begin{bmatrix} 1 & 0 \\ 0 & 0 \end{bmatrix}$ represents an equivalent linear polarizer along the x direction, since only the light wave along the x direction is modulated at and transmitted through the PM. Again, $J_n(\beta)$ is the Bessel function given in Eq.(4-8).

By applying the self-consistency condition, $E'_{1A} = E_{1A}$ and $E'_{1A} = E_{1A}$, and substituting the complex amplitudes of electric field at point B into Eq. (4-9a) and (4-9b), the complex amplitudes in the steady state are given by

$$E_{1x} = \alpha G(E_{1x}, E_{2x}) \left\{J_0(\beta) \cos^2(\theta) E_{1x} + J_{-1}(\beta) \sin^2(\theta) E_{2x}\right\}, \tag{4-10a}$$

$$E_{2x} = \alpha G(E_{1x}, E_{2x}) \left\{J_0(\beta) \sin^2(\theta) E_{2x} + J_1(\beta) \cos^2(\theta) E_{1x}\right\}. \tag{4-10b}$$

In (4-10a), the first term in the braces corresponds to the remained zero-order light wave at λ_1 and the second term represents the contribution of the injected sideband from λ_2. In (4-10b), the first term in the braces corresponds to the remained zero-order light wave at λ_2 and the second term represents the contribution of the injected sideband from λ_1. Such mutual injection locking will help stabilize the dual-wavelength operation.

The mutual injection locking to stabilize the dual wavelength lasing is simulated. In the simulation, the incident angle to the PM-PSFBG is set at two different values, $\theta = \pi/4$ and $\theta = \pi/6$. The power of λ_1 is set to be 20 dB stronger than that of λ_2 in the initial condition. The simulation results are shown in Fig. 4-4. As can be seen from the figure, the two wavelengths reach a steady state after several round trips for both cases.

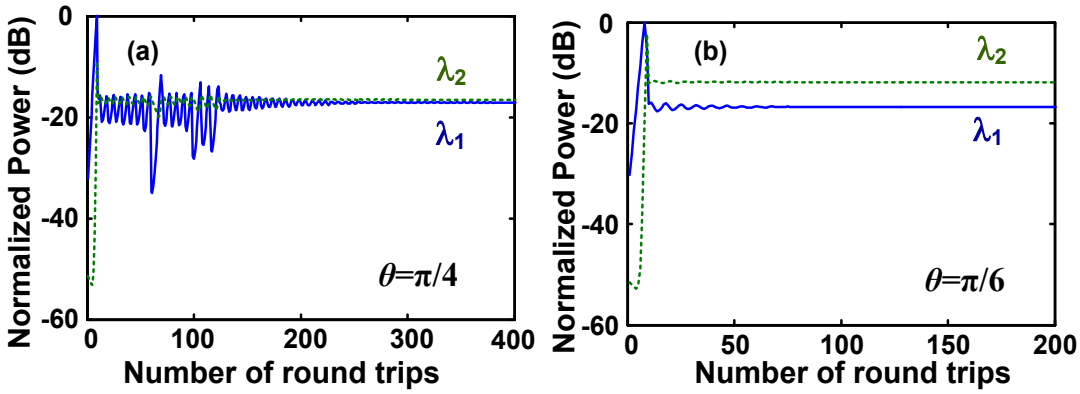

Fig. 4-4. Simulation results. (a) The normalized optical powers for λ_1 (solid line) and λ_2 (dashed line) versus the number of round trips, with an incident angle of $\theta = \pi/4$. (b) The normalized optical powers for λ_1 (solid line) and λ_2 (dashed line) versus the number of round trips, with an incident angle of $\theta = \pi/6$.

It can be seen that in the first few round trips, the higher initial power of λ_1 will make its power increase and the power of λ_2 decrease dramatically due to the mode competition. However, immediately after the first few round trips, in the next tens of round trips, the nonlinear effect of the modulation and OEO injection restrain the mode competition and bring up the power of λ_2: the decreasing optical power at λ_2 will reduce its -1st order

sideband accordingly, which will lead to the reduction in the optical power injected into λ_1. Simultaneously, the increasing λ_1 will induce a stronger injection to λ_2, which counteracts the effect of mode competition. Such reciprocating power vibration of the two wavelengths will finally reach a steady state with a power ratio between the two wavelengths depending on the incident angle θ. Such effect induced by the mutual injection can improve the system stability with an increased tolerance to an imbalanced initial condition.

4.1.5 Transverse load sensing

Since a very stable dual-wavelength lasing is reached, the fiber ring laser can be used for sensing applications. The frequency of the microwave signal generated in the OEO-coupled dual-wavelength laser is only determined by the spacing between the dual wavelengths, which is a function of the birefringence of the PM-PSFBG. If a transverse load is applied to the PM-PSFBG, the beat frequency between the two wavelengths will shift due to the change in the birefringence. Recall the Eq. (3-16), the frequency spacing between the two notches along the two principal axes is given by

$$\Delta\omega = \omega_x - \omega_y = \frac{2cn_0^2\left(p_{11}-p_{12}\right)\left(1+\nu_{\mathrm{p}}\right)\cos\left(2\theta\right)F}{\pi r E \lambda_0}, \tag{4-10}$$

where ω_1, ω_2 are the frequencies corresponding to λ_1 and λ_2, n_0 is the averaging refractive index of the fiber, p_{11} and p_{12} are the components of the strain-optical tensor of the optical material, ν_{p} is Poisson's ratio, ε is the Young's modulus of the fiber, r is the radius of the fiber, φ is the angle between the direction of the force and the slow axis of the fiber, and F is the linear transverse load (force per unit length). By measuring the frequency of the microwave signal, the transverse force applied to the fiber can be interrogated. It is

noteworthy to mention that the sensitivity of the transverse load sensor is directly related to the angle of the force applied to the fiber. Only when the angle of force is 0 or $\pi/2$, in other words, the direction of the force is aligned with either the slow or fast axis of the fiber, a maximum sensitivity can be reached.

4.2 Experiment

In the experiment, we first study the operation of the proposed dual-wavelength fiber ring laser incorporating an injection-coupled OEO. Then, its application for high-resolution and high-speed transverse load sensing is investigated.

4.2.1 Optical carrier generation

We first demonstrate the fiber ring laser to operate for the generation of a single wavelength and dual wavelengths optical carrier. The ultra-narrow transmission bands of the PM-PSFBG are used to select the lasing wavelengths. The PM-PSFBG is fabricated in a PMF using a chirped phase mask that is illumined by a UV light. The phase shift is introduced by laterally moving the phase mask. The transmission and the reflection spectra of the PM-PSFBG along the two principal axes are measured by an optical vector analyzer (OVA, LUNA Technologies) which are shown in Fig. 4-5. As can be seen the PM-PSFBG has a reflectivity over 99.99% for the two reflection bands. In Fig. 4-5(a), the bottom of the transmission spectra has a step, which is caused by a slight misalignment of the polarization direction of the incident light to one principal axis, leading the coupling of the light to the direction of the other principal axis. In the reflection spectra, shown in Fig. 4-5(b), the narrow notches cannot be resolved due to log scale coordinates. The 3-dB reflection bandwidths of the PM-PSFBG along the two principal axes are measured to be 117.3 GHz and 113.3 GHz.

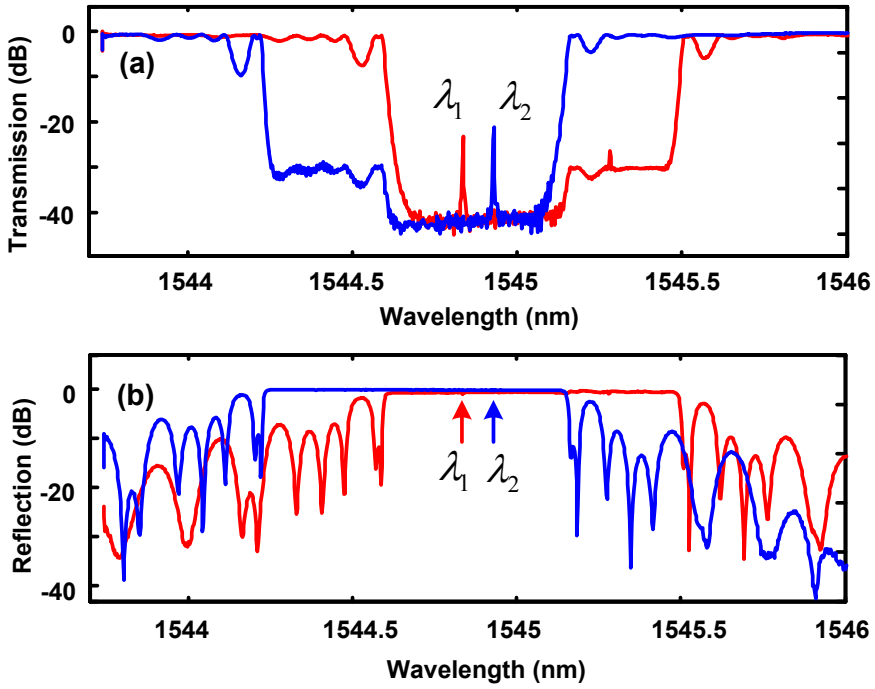

Fig. 4-5 (a) The normalized transmission spectra of the PM-PSFBG along the two principal axes. (b) The normalized reflection spectra of the PM-PSFBG along the two principal axes.

To guarantee that the laser is operating at the narrow transmission bands of the PM-PSFBG, an optical bandpass filter (OBPF, Finisar WaveShaper 4000S) of a bandwidth of 50 GHz is inserted in the fiber ring loop to select the two transmission bands, as shown in Fig. 4-1. If the gain provided by the EDFA (Nortel FA17UFAC-119C28) is sufficiently large to fully compensate for the loss in the fiber ring loop, including the polarization induced coupling loss at the PM-PSFBG, the laser will start to lase. The minimum output power of the EDFA to ensure stable lasing is 11 dBm. In the experiment, to generate a microwave signal with a good signal to noise ratio (SNR) at the output of the PD, the output power of the EDFA is set to be 15 dBm. In this case, the output power of the laser is measure to be -3 dBm.

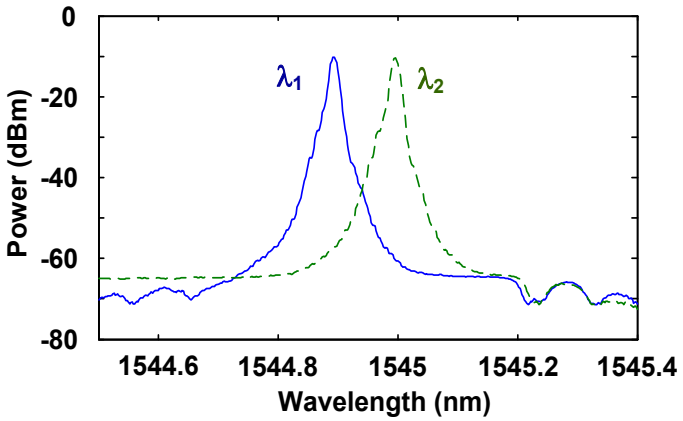

Fig. 4-6. The optical spectrum of the light wave generated by the fiber ring laser at λ_1 (solid line) or λ_2 (dashed line).

As shown in Eq. (4-2), depending on the polarization direction of the light wave relative to the fast axis of the PM-PSFBG, the laser can operate at a single wavelength or dual wavelengths. For example, if the incident angle θ is tuned to be equal to 0^o or 90^o, the transmission of λ_1 or λ_2 is maximized, and the laser will operate at a single wavelength at λ_1 or λ_2. If the incident angle θ is tuned to balance the transmissions at λ_1 and λ_2, then the laser will operate at dual wavelengths. Note that the tuning is done by changing PC1 in the experiment. Fig. 4-6(a) shows the spectrum at the output of the fiber ring laser corresponding to a single wavelength operation at λ_1 or λ_2. As can be seen the two wavelengths are at 1544.895nm and 1544.993 nm with a wavelength spacing of 0.098 nm and a sideband suppression ratio of 50 dB for both wavelengths. To verify that the laser is operating in single longitudinal mode, we apply the light wave from the fiber ring laser to a PD and monitor the spectrum using an electrical spectrum analyzer (ESA). No beat notes are observed which confirms that the fiber ring laser is operating in single longitudinal mode. In the measurement, the loop length of the fiber laser is about 50 m. Note that the single longitudinal mode will not be maintained if the loop length is increased to 500 m. In the experiment, if the loop length is increased greater than 500 m, severe mode hopping and

multiple longitudinal modes would be observed, although the total output power of the laser is kept unchanged.

4.2.2 OEO operation with a single optical carrier

The OEO operation with a single wavelength optical carrier from the fiber ring laser is investigated. The incident angle θ is controlled such that the ring laser is operating at a single wavelength, which is coupled into the OEO loop to serve as the optical carrier. In the experiment, we tune the incident angle θ via changing PC1 to make the laser operate at λ_1 of 1544.895 nm. Due to the PM-IM conversion at the PM-FSFBG, the phase-modulated signal is converted to an SSB+C signal [27], which is detected by the PD (New Focus 10058B, 20 GHz). The optical spectrum of the SSB+C signal is measured by an optical spectrum analyzer (OSA, ANDO 6317B), which is shown in Fig. 4-7.

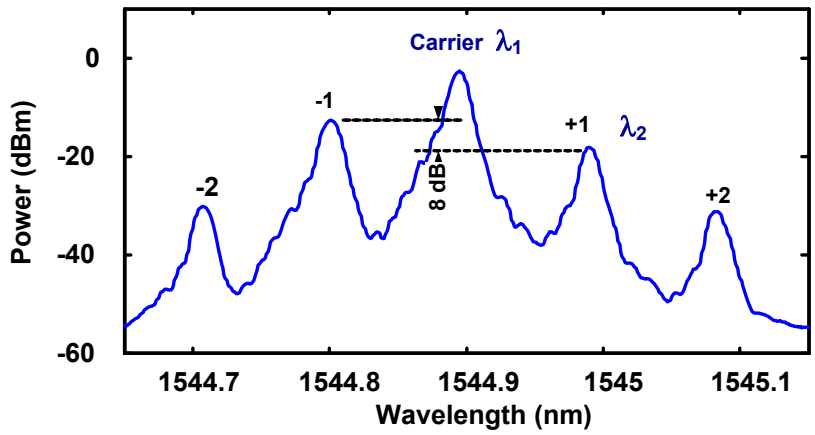

Fig. 4-7 The optical spectrum of the SSB+C signal measured at the Port 3 of the optical circulator (OC) by the OSA. The +1st order sideband is suppressed by 8 dB.

As can be seen the +1st order sideband at 1544.993 nm is suppressed by 8 dB. The detected electrical signal is sent to the EA (6-18 GHz, NARDA 60583). After amplification by the EA, the electrical signal is sent back to the PM to close the OEO loop.

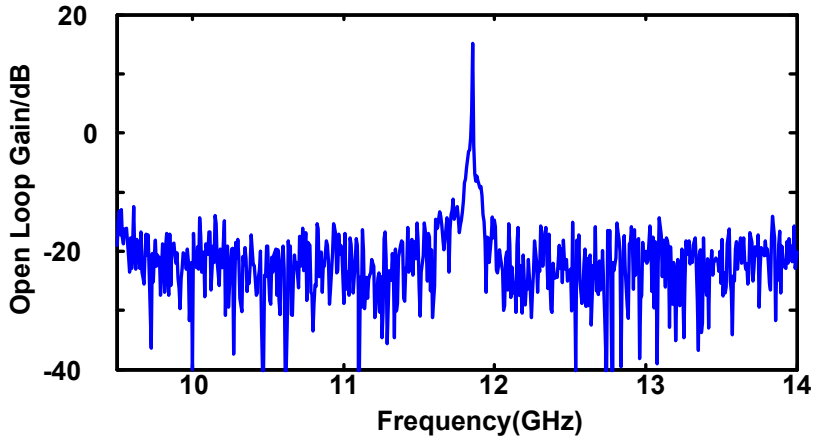

Fig. 4-8 The magnitude response of the equivalent microwave photonic filter.

The joint operation of the PM and the PM-PSFBG is equivalent to a polarization dependent microwave photonic filter. The frequency response of the equivalent microwave photonic filter is measure by a vector network analyzer (VNA, Agilent E8364A), which is shown in Fig. 4-8. As can be seen the microwave photonic filter has a passband centered at 11.8 GHz with a bandwidth of about 10 MHz. Thanks to the ultra-narrow passband of the equivalent microwave photonic filter, a single-frequency oscillation in the OEO is achieved.

4.2.3 OEO operation with dual optical carriers

The OEO operation with two wavelengths from the fiber ring laser is then investigated. The incident angle θ is controlled such that the fiber ring laser is operating at dual wavelengths. The optical spectrum measured at the port 3 of the optical circulator is shown in Fig. 4-9. As can be seen, each wavelength serving as an optical carrier to generate a double-sideband plus carrier (DSB+C) signal. Note that the DSB+C signal for the optical carrier at λ_1 has its +1st order sideband located at the optical carrier at λ_2, and the DSB+C signal for the optical carrier at λ_2 has its -1st order sideband located at the optical carrier at

λ_1. This is the mutual coupling, which is the key mechanism that ensures a stable operation of the dual-wavelength fiber ring laser. Thanks to this mechanism, the injection counteracts the effect of mode competition and stabilizes the dual-wavelength lasing.

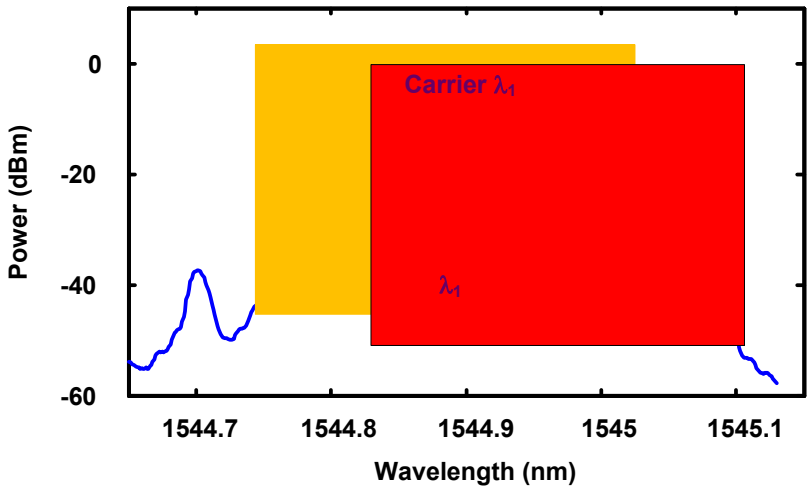

Fig. 4-9. The optical spectrum at the output of port 3 of the optical circulator when the fiber ring laser is operating to generate dual wavelengths.

4.2.4 Microwave signal generation

For the fiber ring laser to operate at both the single-wavelength and the dual-wavelength states, a microwave signal is generated by the OEO. Since the oscillating frequency is only determined by the birefringence of the PM-PSFBG, the frequency of the microwave signal is independent of the wavelength of the optical carrier or carriers from the fiber ring laser. However, the microwave signal generated, when the fiber ring laser is operating in the dual-wavelength state, has better signal quality. The reason lies in that the beating between the two optical carriers provides higher signal power than the beating between the carrier and one sideband. Thus, the fiber ring laser is controlled to operate in the dual-wavelength state to perform the microwave signal generation experiment. By

beating the two lasing wavelengths at the PD, a microwave signal at 11.8 GHz is generated. Note that the frequency of 11.8 GHz corresponds to the intrinsic birefringence of the PM fiber. Fig. 4-10 shows the spectrum of the generated microwave signal. The signal power can reach -3 dBm with a signal-to-noise ratio (SNR) over 50 dB, which can be easily detected and tracked by an electrical spectrum analysis device such as an ESA. A zoom-in view of the spectrum is shown as an inset in Fig. 4-10, which confirms the single-mode oscillation with a sidemode suppression ratio over 50 dB. The free spectrum range (FSR) is measured to be 3.08 MHz, which is consistent with the total length OEO loop of about 60 m. The second peak at 23.6 GHz, shown in Fig. 4-10, is the 2nd harmonic microwave signal generated due to nonlinearity of the OEO loop.

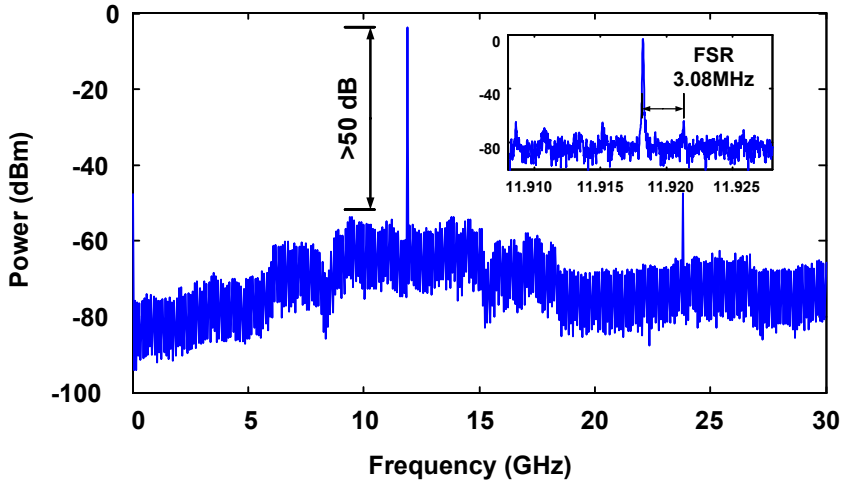

Fig. 4-10. The electrical spectrum of the microwave signal at the output of the PD.

4.2.5 Transverse load sensing

Considering the better quality of the microwave signal generated by the OEO for the fiber ring laser operating at the dual wavelength mode, in the experiment the fiber ring laser is configured to operate at the dual-wavelength mode to perform the sensing experiment.

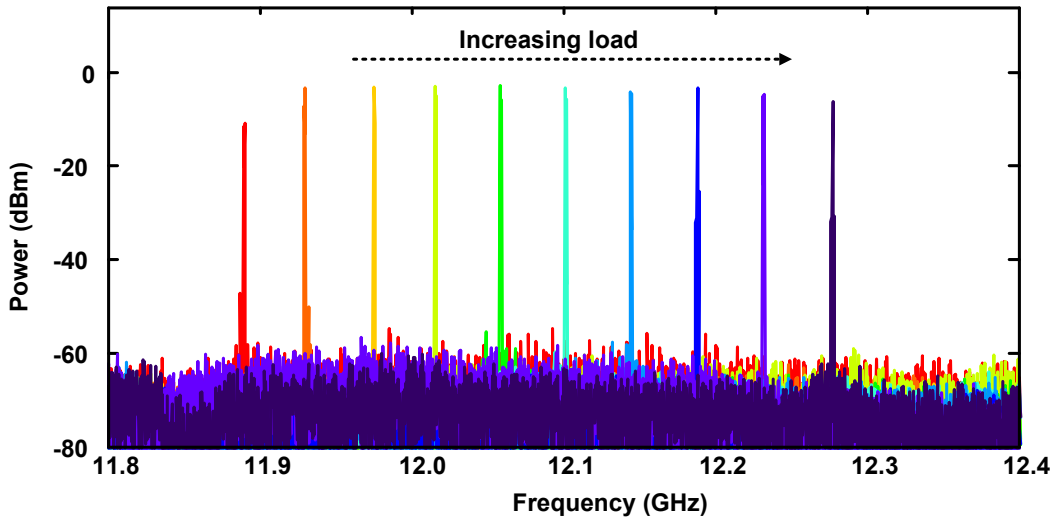

Fig. 4-11. (a) The setup for applying a transverse load to the PM-PSFBG; (b) The electrical spectrum of the microwave signal with increasing the load applied to the slow axis of the PM-PSFBG.

A transverse load is applied to the PM-PSFBG through a glass plate. In the experiment, to ensure the system to reach its highest sensitivity, the transverse load is applied to the PM-PSFBG along its fast or slow axis. A supporting fiber with an identical radius is placed in parallel with the PM-PSFBG to guarantee that the load is applied to the PM-PSFBG transversely, while sharing half of the applied load. To avoid non-uniformed mechanical elastic property of the post coating on the PM-PSFBG, an initial load is applied to the sensing probe in order to reach its linear response regime, which also helps to fix the fiber with a constant angle to the direction of the force when increasing or decreasing the load. By increasing the load applied to the PM-PSFBG, the beat frequency is shifted towards a higher frequency, as shown in Fig. 4-11, measured by an ESA, from 11.9033 to 12.3897 GHz with a load from 0 to 0.0397 N/mm.

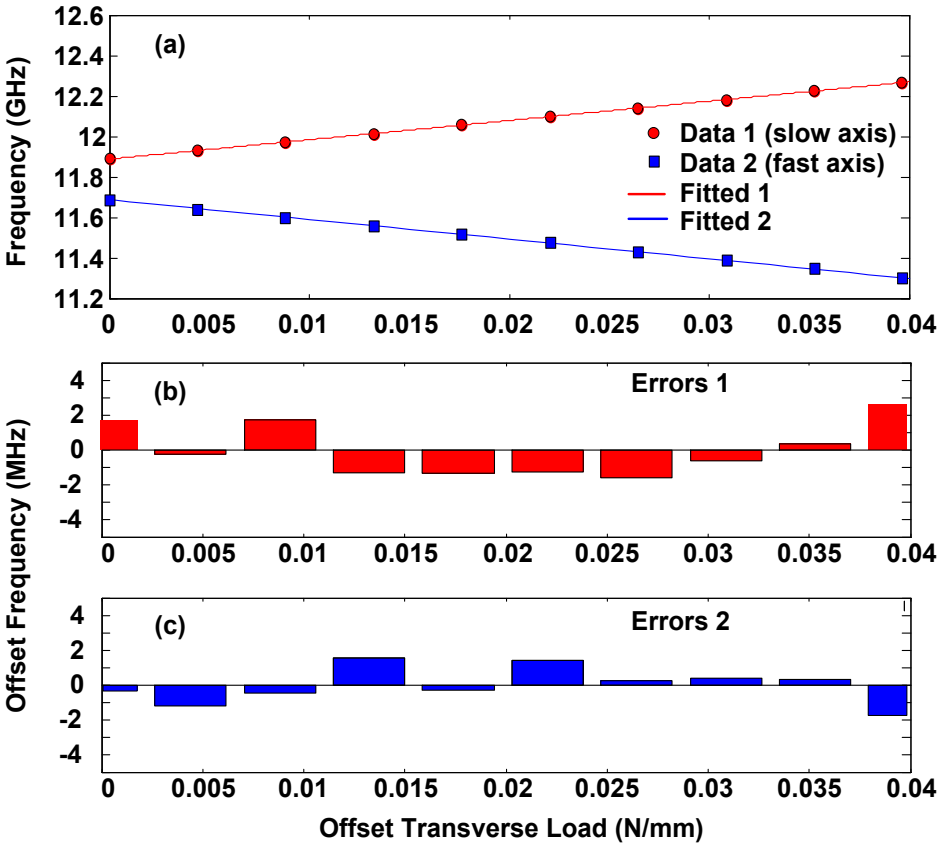

Fig. 4-12. (a) The measured microwave frequencies versus the transverse load along the slow axis (data1) and fast axis (data 2); (b) The errors between the measured frequencies and the linearly fitted curve along the fast axis of the PM-PSFBG; (c) the errors between the measured frequencies and the linearly fitted curve along the slow axis of the PM-PSFBG.

According the theoretical analysis in Section 4.1.5, the frequency of the beat note is linearly proportional to the load applied to the fiber with a given angle between the force direction and the principal axis. The microwave frequency with the force applied along either the slow or the fast axis of the PM-PSFBG is measured. To do so, we first apply the force along the slow axis of the PM-PSFBG. By increasing the force with a constant force increment of 0.0044 N/mm, the frequencies are measured and shown in Fig. 4-12(a) as solid squares. A linearly fitted curve is also shown. Then, we apply the force along the fast axis of the PM-PSFBG. Again, the force is increased with a constant force increment of 0.0044 N/mm. The frequencies are measured and shown in Fig. 4-12(a) as solid circles.

The frequency separation at a zero load is caused by the initial load applied to the PM-PSFBG. By using the typical values of a silica fiber at a wavelength of 1550 nm: $n_0 = 1.467$, $p_{11} = 0.12$, $p_{12} = 0.27$, $v_p = 0.17$, $E = 7.6\times104$ N/mm and the radius of optical fiber $r = 62.5$ m, the theoretical sensitivity of the sensor is calculated to be 9.6 GHz/(N/mm), while the linearly fitted slopes are +9.757 GHz/ (N/mm) and -9.735 GHz/ (N/mm) for the force applied along the fast and the slow axes, respectively. A good agreement between the theoretical and the experimental results is reached. The errors between the measured frequencies and the linearly fitted values, shown in Fig. 4-12(b) and (c), are all smaller than 3.08 MHz, which is within one FSR of the OEO loop. This illustrates that the microwave signal will oscillate at the discrete frequencies determined by the FSR which is close to the theoretical value where only the birefringence is taken into consideration. Therefore, the resolution of the system can be defined by the FSR of the OEO loop. The resolution of the system is calculated as 3.1566×10^{-4}N/mm or 3.1638×10^{-4}N/mm, corresponding the FSR of 3.08 MHz, for the force applied along, respectively, the fast and slow axes in the experiment.

The measurement range of the optical probe can reach 7.5 N/mm, based on the spectral width from the ultra-narrow notch to one edge of its reflection band, which is about 75 GHz. The measurement range is also limited by the bandwidths of the PD, the PM and the EA. In the experiment, the measurement range is ~0.6N/mm, limited by the bandwidth of the EA (6-18 GHz) and the PM-PSFBG initial-birefringence-induced offset frequency (11.8 GHz)

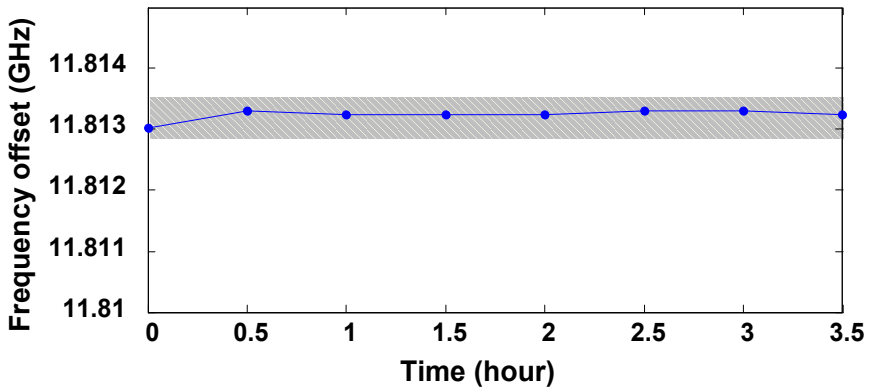

Fig. 4-13. Stability test result: frequency measurement with 0.5 hour interval for a temporal duration of 3.5 hours.

The stability of the sensor is also studied. To do so, we measure the microwave frequency every half an hour during a 3.5 hours period without a load applied to the fiber. This is the condition under which the fiber sensor suffers from the strongest influence from the environment disturbance. As can be seen from the results shown in Fig. 4-13, the frequency fluctuations are always within 0.5 MHz. Considering the FSR of the OEO loop is 3.08 MHz and the bandwidth of the equivalent microwave photonic filter is 10 MHz, thus the filter is able to select a single mode to guarantee a single mode operation. In the experiment, no mode hoping is observed. The fluctuations are mainly caused by the environmental disturbance such as vibrations, air turbulence and temperature fluctuations. In the experiment, all fibers including the PM-PSFBG are exposed to the environment with no packaging. The errors can be reduced if the system is well packaged with temperature control.

In the experiment, the PM-PSFBG is fabricated using a polarization maintaining fiber (PMF), which has an initial birefringence, leading to a non-zero beat frequency at 11.8 GHz. If the PM-PSFBG is replaced by a PSFBG written in a fiber with a much smaller initial

birefringence, a much lower beat frequency will be generated. Thus, the interrogation system can be implemented using low-frequency electronic components with reduced cost.

4.3 Summary

A novel dual-wavelength fiber ring laser with improved lasing stability realized through the use of an injection-coupled OEO was proposed and demonstrated, and its application to transverse load sensing was studied. The key mechanism to increase the lasing stability is to use the microwave signal from the OEO to injection lock the dual wavelengths of the fiber ring laser. A theoretical analysis was performed, which was verified by an experiment.

Thanks to the significantly increased stability, the fiber ring laser is an excellent candidate for sensing applications. In the experiment, a transverse load was applied to the PM-PSFBG, and the microwave frequencies for different transverse load were measured. The experimental results showed that the theoretical and the experimental results agreed well. The sensitivity of the transverse load sensor was measured as high as +9.757 GHz/(N/mm) and -9.735 GHz/(N/mm), when the load was applied along the fast and slow axes, respectively. The high frequency purity and stability of the generated microwave signal enabled high accuracy and always valid measurement and the time-domain frequency interrogation allowed the system to operate at an ultra-high speed.

Chapter 5

Conclusion and Discussion

5.1 Conclusion

The proposed dual-frequency OEO initiated the study on this new type of polarization dependent hybrid oscillator. To obtain two orthogonally polarized light waves in the OEO loop, a PM-PSFBG is employed in the OEO loop to create two orthogonally polarized notches, which leads to the generation of two oscillating frequencies. Both the theoretical and experimental results demonstrated that the multiple non-harmonic microwave signals and their beat note can be simultaneously supported inside the OEO loop. Comparing to commonly known multi wavelength laser, the electrical amplification in OEO can effectively avoid the inter-mode competition induced by the homogeneous optical gain saturation and improve the stability of the oscillator. The optical energy distribution along the two principle axes can be tuned by controlling the azimuth angle of the incident pump light. The beat note generated by the nonlinearity of the PD can be used to demodulate the transverse strain applied on the grating. A fiber-optic sensor with frequency interrogation was implemented by proposed dual-frequency OEO with a sensitivity of 9.73 GHz/(N/mm).

To further refine the sensor system and remove the ambiguity in the frequency measurement, a fiber ring laser coupled dual-frequency OEO is proposed. The dual-frequency OEO can operate with two stable optical carrier and output a single microwave frequency which is determined by the fiber birefringence. Due to the re-injection of the transmitted light from PM-PSFBG, the stability and the output power of the microwave signal can be significantly enhanced. A theoretical model of the mechanism to setup the steady state has been developed in terms of the complex amplitude of the electric fields

associated with the two wavelengths. The transition process before the steady state was established illustrated the stabilizing effect of the optoelectronic feedback. To the best of our knowledge, the nonlinearities in the proposed model introduced by the phase modulator and the optical gain medium are both characterized in the iterative equations for the first time. The system is experimentally demonstrated to be able to stably run with either only one carrier or two carriers. A transverse load sensing demonstration based on this dual wavelength laser coupled OEO was performed, which presented a promising prospect in transverse load sensing with an enhanced validity. Since there was only the signal with beat frequency oscillating in the loop, the ambiguity of the between the beat and the oscillating frequencies can be avoided.

5.2 Discussion

The two configurations proposed in Chapter 3 and Chapter 4 have several interesting and unique nonlinear characteristics which can be further exploited in the future. Meanwhile, optimizing the sensor probe and integrating the bulky optical and electronics devices in the experiment may help to commercialize the proposed sensor system.

For the dual-frequency optoelectronic oscillator setup proposed in Chapter 3, the operation with multiple non-harmonic frequencies has been experimentally demonstrated. Further investigation on the theoretical model of this operation can provide additional insights of the nonlinear behaviors of the dual-frequency OEO under different conditions. The two passbands in the two polarization states enrich the system's nonlinearities and the coupling between the two non-harmonic longitudinal modes will possibly lead into different dynamical regimes.

Regarding the configuration in Chapter 4, a preliminary steady state modeling has been given in terms of the amplitudes of the two lasing wavelengths. However, we can expect more complex behavior to occur in the system. For example, the coupling between the two polarization states may create vector solitons in the hybrid loop, which reproduce themselves after each round trip. In order to improve the performance of the sensor and reduce the total cost, the system can be further exploited in three possible aspects: 1) The sensor probe may be optimized to obtain higher sensitivities by employing the micro structure optical fibers. The increased responsivity to anisotropic strain or other external disturbances also provide an alternative way to generate widely tunable microwave signals. 2) Instead of using the EDFA, the optical gain can be provided by mature semiconductor optical amplifiers (SOA) which have the potential to be integrated with low cost. 3) The

spectrum resolved interrogation can be achieved in time domain using sampling electronic devices. This will simplify the current interrogation units and reduce the cost for the whole system. 4) The modulation is possible to be realized by directly modulating the external laser, which reduces the cost on the optoelectronic modulator.

BIBLIOGRAPHY

[1] A. J. Seeds and K. J. Williams, "Microwave photonics," *IEEE/OSA J. Lightw. Technol.,* vol. 24, no. 12, pp. 4628-4641, Dec. 2006.

[2] J. Capmany and D. Novak, "Microwave photonics combines two worlds," *Nature Photon.,* vol. 1, no. 6, pp. 319-330, Jun. 2007.

[3] J. P. Yao, "Microwave Photonics," *IEEE/OSA J. Lightw. Technol.,* vol. 27, no. 1-4, pp. 314-335, Jan-Feb. 2009.

[4] H. Al-Raweshidy and S. Komaki, *Radio over Fiber Technologies for Mobile Communications Networks*. Boston: Artech House, 2002.

[5] F. Zeng and J. P. Yao, "An approach to ultrawideband pulse generation and distribution over optical fiber," *IEEE Photon. Technol. Lett.,* vol. 18, no. 5-8, pp. 823-825, Mar-Apr. 2006.

[6] A. G. Larrode, A. M. J. Koonen, J. J. V. Omos, and A. Ng'Oma, "Bidirectional radio-over-fiber link employing optical frequency multiplication," *IEEE Photon. Technol. Lett.,* vol. 18, no. 1-4, pp. 241-243, Jan-Feb. 2006.

[7] J. Capmany, B. Ortega, and D. Pastor, "A tutorial on microwave photonic filters," *IEEE/OSA J. Lightw. Technol.,* vol. 24, no. 1, pp. 201-229, Jan. 2006.

[8] J. Capmany, D. Pastor, A. Martinez, B. Ortega, and S. Sales, "Microwave photonic filters with negative coefficients based on phase inversion in an electro-optic modulator," *Opt. Lett.,* vol. 28, no. 16, pp. 1415-1417, Aug. 2003.

[9] A. Loayssa, J. Capmany, M. Sagues, and J. Mora, "Demonstration of incoherent microwave photonic filters with all-optical complex coefficients," *IEEE Photon. Technol. Lett.,* vol. 18, no. 13-16, pp. 1744-1746, Jul-Aug. 2006.

[10] E. Hamidi, D. E. Leaird, and A. M. Weiner, "Tunable programmable microwave photonic filters based on an optical frequency comb," *IEEE Trans. Microw. Theory Tech.,* vol. 58, no. 11, pp. 3269-3278, Nov. 2010.

[11] W. Z. Li and J. P. Yao, "Investigation of photonically assisted microwave frequency multiplication based on external modulation," *IEEE Trans. Microw. Theory Tech.,* vol. 58, no. 11, pp. 3259-3268, Nov. 2010.

[12] A. Wiberg, P. Perez-Millan, M. V. Andres, and P. O. Hedekvist, "Microwave-photonic frequency multiplication utilizing optical four-wave mixing and fiber

Bragg gratings," *IEEE/OSA J. Lightw. Technol.,* vol. 24, no. 1, pp. 329-334, Jan. 2006.

[13] C. K. Sun, R. J. Orazi, and S. A. Pappert, "Efficient microwave frequency conversion using photonic link signal mixing," *IEEE Photon. Technol. Lett.,* vol. 8, no. 1, pp. 154-156, Jan. 1996.

[14] R. Slavik, Y. Park, N. Ayotte, S. Doucet, T. J. Ahn, S. LaRochelle*, et al.*, "Photonic temporal integrator for all-optical computing," *Opt. Express,* vol. 16, no. 22, pp. 18202-18214, Oct. 2008.

[15] A. Loayssa and F. J. Lahoz, "Broad-band RF photonic phase shifter based on stimulated Brillouin scattering and single-sideband modulation," *IEEE Photon. Technol. Lett.,* vol. 18, no. 1-4, pp. 208-210, Jan-Feb. 2006.

[16] F. F. Liu, T. Wang, L. Qiang, T. Ye, Z. Y. Zhang, M. Qiu*, et al.*, "Compact optical temporal differentiator based on silicon microring resonator," *Opt. Express,* vol. 16, no. 20, pp. 15880-15886, Sep 29. 2008.

[17] M. H. Asghari and J. Azana, "All-optical Hilbert transformer based on a single phase-shifted fiber Bragg grating: design and analysis," *Opt. Lett.,* vol. 34, no. 3, pp. 334-336, Feb. 2009.

[18] J. P. Yao, F. Zeng, and Q. Wang, "Photonic generation of ultrawideband signals," *IEEE/OSA J. Lightw. Technol.,* vol. 25, no. 11, pp. 3219-3235, Nov. 2007.

[19] T. M. Fortier, M. S. Kirchner, F. Quinlan, J. Taylor, J. C. Bergquist, T. Rosenband*, et al.*, "Generation of ultrastable microwaves via optical frequency division," *Nature Photon.,* vol. 5, no. 7, pp. 425-429, Jul. 2011.

[20] M. G. Tylor, "Coherent detection method using DSP for demodulation of signal and subsequent equalization of propagation impairments," *IEEE Photon. Technol. Lett.,* vol. 16, no. 2, pp. 674-676, Feb. 2004.

[21] X. Li, X. Chen, G. Goldfarb, E. Mateo, I. Kim, F. Yaman*, et al.*, "Electronic post-compensation of WDM transmission impairments using coherent detection and digital signal processing," *Opt. Express,* vol. 16, no. 2, pp. 880-888, Jan. 2008.

[22] J. Armstrong, "OFDM for Optical Communications," *IEEE/OSA J. Lightw. Technol.,* vol. 27, no. 1-4, pp. 189-204, Jan-Feb. 2009.

[23] X. S. Yao and L. Maleki, "Converting light into spectrally pure microwave oscillation," *Opt. Lett.,* vol. 21, no. 7, pp. 483-485, Apr 1. 1996.

[24] G. R. Huggett, "Mode-locking of CW lasers by regenerative RF feedback," *Appl. Phys. Lett.,* vol. 13, no. 5, pp. 186-187, Sep. 1968.

[25] K. Koizumi, M. Yoshida, T. Hirooka, and M. Nakazawa, "10 GHz, 1.1 ps optical pulse generation from a regeneratively mode-locked Yb fiber laser in the 1.1 mu m band," *Opt. Express,* vol. 19, no. 25, pp. 25426-25432, Dec. 2011.

[26] T. Erneux, A. Gavrielides, and M. Sciamanna, "Stable microwave oscillations due to external-cavity-mode beating in laser diodes subject to optical feedback," *Phys. Rev. A,* vol. 66, no. 3, Sep. 2002.

[27] J. P. Zhuang and S. C. Chan, "Tunable photonic microwave generation using optically injected semiconductor laser dynamics with optical feedback stabilization," *Opt. Lett.,* vol. 38, no. 3, pp. 344-346, Feb. 2013.

[28] M. Haji, L. P. Hou, A. E. Kelly, J. Akbar, J. H. Marsh, J. M. Arnold*, et al.*, "High frequency optoelectronic oscillators based on the optical feedback of semiconductor mode-locked laser diodes," *Opt. Express,* vol. 20, no. 3, pp. 3268-3274, Jan. 2012.

[29] C. Y. Lin, F. Grillot, Y. Li, R. Raghunathan, and L. F. Lester, "Microwave characterization and stabilization of timing jitter in a quantum-dot passively mode-locked laser via external optical feedback," *IEEE J. Sel. Topics Quantum Electron.,* vol. 17, no. 5, pp. 1311-1317, Sep-Oct. 2011.

[30] P. Bouyer, T. L. Gustavson, K. G. Haritos, and M. A. Kasevich, "Microwave signal generation with optical injection locking," *Opt. Lett.,* vol. 21, no. 18, pp. 1502-1504, Sep 15. 1996.

[31] R. P. Braun, G. Grooskopf, D. Rohde, and F. Schmidt, "Low-phase-noise millimeter-wave generation at 64 GHz and data transmission using optical sideband injection locking," *IEEE Photon. Technol. Lett.,* vol. 10, no. 5, pp. 728-730, May. 1998.

[32] S. C. Chan, "Analysis of an Optically Injected Semiconductor Laser for Microwave Generation," *IEEE J. Quantum Electron.,* vol. 46, no. 3, pp. 421-428, Mar. 2010.

[33] S. C. Chan and J. M. Liu, "Tunable narrow-linewidth photonic microwave generation using semiconductor laser dynamics," *IEEE J. Sel. Topics Quantum Electron.,* vol. 10, no. 5, pp. 1025-1032, Sep-Oct. 2004.

[34] X. S. Yao and L. Maleki, "Optoelectronic microwave oscillator," *J. Opt. Soc. Am. B,* vol. 13, no. 8, pp. 1725-1735, Aug. 1996.

[35] W. M. Zhou and G. Blasche, "Injection-locked dual opto-electronic oscillator with ultra-low phase noise and ultra-low spurious level," *IEEE Trans. Microw. Theory Tech.,* vol. 53, no. 3, pp. 929-933, Mar. 2005.

[36] OEwaves, Inc.. (2014 Feb.). *Compact Opto-Electronic Oscillator (COEO)* [Online]. Available: http://www.oewaves.com/compact-oeo-sp-1149514981

[37] L. Larger and J. M. Dudley, "Nonlinear Dynamics Optoelectronic Chaos," *Nature,* vol. 465, no. 7294, pp. 41-42, May. 2010.

[38] K. E. Callan, L. Illing, Z. Gao, D. J. Gauthier, and E. Scholl, "Broadband Chaos Generated by an Optoelectronic Oscillator," *Phys. Rev. Lett.,* vol. 104, no. 11, Mar. 2010.

[39] W. Li, F. Kong, and J. Yao, "Arbitrary microwave waveform generation based on a tunable optoelectronic oscillator," *IEEE/OSA J. Lightw. Technol.,* vol. 31, no. 23, pp. 3780-3786, Dec. 2013.

[40] H. Tsuchida and M. Suzuki, "40-Gb/s optical clock recovery using an injection-locked optoelectronic oscillator," *IEEE Photon. Technol. Lett.,* vol. 17, no. 1, pp. 211-213, Jan. 2005.

[41] X. S. Yao and G. Lutes, "A high-speed photonic clock and carrier recovery device," *IEEE Photon. Technol. Lett.,* vol. 8, no. 5, pp. 688-690, May. 1996.

[42] X. S. Yao and L. Maleki, "Multiloop optoelectronic oscillator," *IEEE J. Quantum Electron.,* vol. 36, no. 1, pp. 79-84, Jan. 2000.

[43] Y. C. Kouomou, P. Colet, L. Larger, and N. Gastaud, "Chaotic breathers in delayed electro-optical systems," *Phys. Rev. Lett.,* vol. 95, no. 20, Nov. 2005.

[44] M. Peil, M. Jacquot, Y. K. Chembo, L. Larger, and T. Erneux, "Routes to chaos and multiple time scale dynamics in broadband bandpass nonlinear delay electro-optic oscillators," *Phys. Rev. E,* vol. 79, no. 2, Feb. 2009.

[45] X. S. Yao, "High-quality microwave signal generation by use of Brillouin scattering in optical fibers," *Opt. Lett.,* vol. 22, no. 17, pp. 1329-1331, Sep. 1997.

[46] W. Z. Li and J. P. Yao, "An optically tunable optoelectronic oscillator," *IEEE/OSA J. Lightw. Technol.,* vol. 28, no. 18, pp. 2640-2645, Sep. 2010.

[47] W. Z. Li and J. P. Yao, "A wideband frequency tunable optoelectronic oscillator incorporating a tunable microwave photonic filter based on a phase-shifted fiber Bragg grating," *Photonics North 2011,* vol. 8007, 2011.

[48] S. L. Pan and J. P. Yao, "Wideband and frequency-tunable microwave generation using an optoelectronic oscillator incorporating a Fabry-Perot laser diode with external optical injection," *Opt. Lett.,* vol. 35, no. 11, pp. 1911-1913, Jun. 2010.

[49] I. Ozdur, D. Mandridis, M. U. Piracha, M. Akbulut, N. Hoghooghi, and P. J. Delfyett, "Optical frequency stability measurement using an etalon-based otoelectronic oscillator," *IEEE Photon. Technol. Lett.,* vol. 23, no. 4, pp. 263-265, Feb. 2011.

[50] M. Li, W. Li, J. Yao, and J. Azana, "Femtometer-Resolution wavelength interrogation of a phase-shifted fiber bragg grating sensor using an optoelectronic oscillator," 2012, p. BTu2E.3.

[51] M. Jones, "Structural-health monitoring: A sensitive issue," *Nature Photon.,* vol. 2, no. 3, pp. 153-154, Mar. 2008.

[52] H. L. Guo, G. Z. Xiao, N. Mrad, and J. P. Yao, "Fiber optic sensors for structural health monitoring of air platforms," *Sensors,* vol. 11, no. 4, pp. 3687-3705, Apr. 2011.

[53] E. Pinet, "Medical applications: Saving lives," *Nature Photon.,* vol. 2, no. 3, pp. 150-152, Mar. 2008.

[54] H. Nakstad and J. T. Kringlebotn, "Oil and gas applications: Probing oil fields," *Nature Photon.,* vol. 2, no. 3, pp. 147-149, Mar. 2008.

[55] N. Imoto, N. Yoshizawa, J. I. Sakai, and H. Tsuchiya, "Birefringence in single-mode optical fiber due to elliptical core deformation and stress anisotropy," *IEEE J. Quantum Electron.,* vol. 16, no. 11, pp. 1267-1271, Nov. 1980.

[56] L. Y. Shao, A. Laronche, M. Smietana, P. Mikulic, W. J. Bock, and J. Albert, "Highly sensitive bend sensor with hybrid long-period and tilted fiber Bragg grating," *Opt. Comm.,* vol. 283, no. 13, pp. 2690-2694, Jul. 2010.

[57] R. Ulrich, S. C. Rashleigh, and W. Eickhoff, "Bending-Induced Birefringence in Single-Mode Fibers," *Opt. Lett.,* vol. 5, no. 6, pp. 273-275, Jun. 1980.

[58] H. Chi, X. M. Tao, D. X. Yang, and K. S. Chen, "Simultaneous measurement of axial strain, temperature, and transverse load by a superstructure fiber grating," *Opt. Lett.,* vol. 26, no. 24, pp. 1949-1951, Dec. 2001.

[59] M. LeBlanc, S. T. Vohra, T. E. Tsai, and E. J. Friebele, "Transverse load sensing by use of pi-phase-shifted fiber Bragg gratings," *Opt. Lett.,* vol. 24, no. 16, pp. 1091-1093, Aug. 1999.

[60] B. O. Guan, L. Jin, Y. Zhang, and H. Y. Tam, "Polarimetric heterodyning fiber grating laser sensors," *IEEE/OSA J. Lightw. Technol.,* vol. 30, no. 8, pp. 1097-1112, Apr. 2012.

[61] J. J. Zhang, Q. Z. Sun, R. B. Liang, J. H. Wo, D. M. Liu, and P. Shum, "Microfiber Fabry-Perot interferometer fabricated by taper-drawing technique and its application as a radio frequency interrogated refractive index sensor," *Opt. Lett.,* vol. 37, no. 14, pp. 2925-2927, Jul. 2012.

[62] X. H. Zou and J. P. Yao, "An optical approach to microwave frequency measurement with adjustable measurement range and resolution," *IEEE Photon. Technol. Lett.,* vol. 20, no. 21-24, pp. 1989-1991, Nov-Dec. 2008.

[63] A. Neyer and E. Voges, "High-frequency electro-optic oscillator using an integrated interferometer," *Appl. Phys. Lett.,* vol. 40, no. 1, pp. 6-8, Jan. 1982.

[64] C. W. Nelson, A. Hati, D. A. Howe, and W. Zhou, "Microwave optoelectronic oscillator with optical gain," in *Frequency Control Symposium, 2007 Joint with the 21st European Frequency and Time Forum. IEEE International*, 2007, pp. 1014-1019.

[65] P. S. Devgan, M. W. Pruessner, V. J. Urick, and K. J. Williams, "Detecting low-power RF signals using a multimode optoelectronic oscillator and integrated optical filter," *IEEE Photon. Technol. Lett.,* vol. 22, no. 3, pp. 152-154, Feb. 2010.

[66] Y. K. Chembo, L. Larger, R. Bendoula, and P. Colet, "Effects of gain and bandwidth on the multimode behavior of optoelectronic microwave oscillators," *Opt. Express,* vol. 16, no. 12, pp. 9067-9072, Jun. 2008.

[67] K. O. Hill, Y. Fujii, D. C. Johnson, and B. S. Kawasaki, "Photosensitivity in optical fiber waveguides: application to reflection filter fabrication," *Appl. Phys. Lett.,* vol. 32, no. 10, pp. 647-649, May 1978.

[68] G. Meltz, W. W. Morey, and W. H. Glenn, "Formation of Bragg Gratings in Optical Fibers by a Transverse Holographic Method," *Opt. Lett.,* vol. 14, no. 15, pp. 823-825, Aug. 1989.

[69] K. O. Hill, B. Malo, F. Bilodeau, D. C. Johnson, and J. Albert, "Bragg Gratings Fabricated in Monomode Photosensitive Optical-Fiber by UV Exposure through a Phase Mask," *Appl. Phys. Lett.,* vol. 63, no. 3, pp. 424-424, Jul. 1993.

[70] E. Udd and W. B. Spillman, "*Fiber Optic Sensors: An Introduction for Engineers and Scientists*, Second Edition," ed: New York: John Wiley & Sons, Inc., 2011.

[71] J. Albert, L. Y. Shao, and C. Caucheteur, "Tilted fiber Bragg grating sensors," *Laser Photon. Rev.,* vol. 7, no. 1, pp. 83-108, Jan. 2013.

[72] X. F. Chen, J. P. Yao, and Z. C. Deng, "Ultranarrow dual-transmission-band fiber Bragg grating filter and its application in a dual-wavelength single-longitudinal-mode fiber ring laser," *Opt. Lett.,* vol. 30, no. 16, pp. 2068-2070, Aug. 2005.

[73] K. O. Hill, F. Bilodeau, B. Malo, T. Kitagawa, S. Theriault, D. C. Johnson*, et al.*, "Chirped in-fiber bragg gratings for compensation of optical-fiber dispersion," *Opt. Lett.,* vol. 19, no. 17, pp. 1314-1316, Sep. 1994.

[74] I. A. Lobach and S. I. Kablukov, "Application of a self-sweeping Yb-doped fiber laser for high-resolution characterization of phase-shifted FBGs," *IEEE/OSA J. Lightw. Technol.,* vol. 31, no. 18, pp. 2982-2987, Sep. 2013.

[75] H. Shahoei and J. P. Yao, "Tunable microwave photonic phase shifter based on slow and fast light effects in a tilted fiber Bragg grating," *Opt. Express,* vol. 20, no. 13, pp. 14009-14014, Jun. 2012.

[76] A. Melloni, M. Chinello, and M. Martinelli, "All-optical switching in phase-shifted fiber Bragg grating," *IEEE Photon. Technol. Lett.,* vol. 12, no. 1, pp. 42-44, Jan. 2000.

[77] I. V. Kabakova, B. Corcoran, J. A. Bolger, C. M. de Sterke, and B. J. Eggleton, "All-optical self-switching in optimized phase-shifted fiber Bragg grating," *Opt. Express,* vol. 17, no. 7, pp. 5083-5088, Mar. 2009.

[78] G. P. Agrawal and S. Radic, "Phase-shifted fiber bragg gratings and their application for wavelength demultiplexing," *IEEE Photon. Technol. Lett.,* vol. 6, no. 8, pp. 995-997, Aug. 1994.

[79] W. Z. Li, M. Li, and J. P. Yao, "A narrow-passband and frequency-tunable microwave photonic filter based on phase-modulation to intensity-modulation conversion using a phase-shifted fiber Bragg grating," *IEEE Trans. Microw. Theory Tech.,* vol. 60, no. 5, pp. 1287-1296, May. 2012.

[80] G. Z. Xiao, P. Zhao, F. G. Sun, Z. G. Lu, Z. Y. Zhang, and C. P. Grover, "Interrogating fiber Bragg grating sensors by thermally scanning a demultiplexer based on arrayed waveguide gratings," *Opt. Lett.,* vol. 29, no. 19, pp. 2222-2224, Oct. 2004.

[81] M. Han, T. Q. Liu, L. L. Hu, and Q. Zhang, "Intensity-demodulated fiber-ring laser sensor system for acoustic emission detection," *Opt. Express,* vol. 21, no. 24, pp. 29269-29276, Dec. 2013.

[82] L. Jin, Y. N. Tan, Z. Quan, M. P. Li, and B. O. Guan, "Strain-insensitive temperature sensing with a dual polarization fiber grating laser," *Opt. Express,* vol. 20, no. 6, pp. 6021-6028, Mar. 2012.

[83] W. Z. Li and J. P. Yao, "A wideband frequency tunable optoelectronic oscillator incorporating a tunable microwave photonic filter based on phase-modulation to intensity-modulation conversion using a phase-shifted fiber Bragg grating," *IEEE Trans. Microw. Theory Tech.,* vol. 60, no. 6, pp. 1735-1742, Jun. 2012.

[84] T. Erdogan, "Fiber grating spectra," *IEEE/OSA J. Lightw. Technol.,* vol. 15, no. 8, pp. 1277-1294, Aug. 1997.

[85] A. D. Kersey, M. A. Davis, H. J. Patrick, M. LeBlanc, K. P. Koo, C. G. Askins*, et al.*, "Fiber grating sensors," *IEEE/OSA J. Lightw. Technol.,* vol. 15, no. 8, pp. 1442-1463, Aug. 1997.

[86] R. Waxler and G. Cleek, "Effect OF temperature and pressure on refractive-index of some oxide glasses," *J. Res. Natl. Stand. Sec. A,* no. 6, pp. 755-763, Aug. 1973.

[87] J. F. Nye, *Physical Properties of Crystals: Their Representation by Tensors and Matrices*. New York: Oxford Science Publications, 1957.

[88] K. L. Johnson, K. Kendall, and A. D. Roberts, "Surface energy and the contact of elastic solids," *Proc. R. Soc. A,* vol. 324, no. 1558, pp. 301-313, Sep. 1971.

[89] P. D. Gianino and B. Bendow, "Calculations of stress-induced changes in the transverse refractive-index profile of optical fibers," *Appl. Opt.,* vol. 20, no. 3, pp. 430-434, 1981.